arXiv:1911.01166v1 [cs.MS] 4 Nov 2019

Abstractions and automated algorithms for mixed domain finite element methods

CÉCILE DAVERSIN-CATTY, Simula Research Laboratory, Norway
CHRIS N. RICHARDSON, BP Institute, University of Cambridge, United Kingdom
ADA J. ELLINGSRUD, Simula Research Laboratory, Norway
MARIE E. ROGNES, Simula Research Laboratory, Norway

Mixed dimensional partial differential equations (PDEs) are equations coupling unknown fields defined over domains of differing topological dimension. Such equations naturally arise in a wide range of scientific fields including geology, physiology, biology and fracture mechanics. Mixed dimensional PDEs are also commonly encountered when imposing non-standard conditions over a subspace of lower dimension e.g. through a Lagrange multiplier. In this paper, we present general abstractions and algorithms for finite element discretizations of mixed domain and mixed dimensional PDEs of co-dimension up to one (i.e. nD-mD with $|n-m| \leqslant 1$). We introduce high level mathematical software abstractions together with lower level algorithms for expressing and efficiently solving such coupled systems. The concepts introduced here have also been implemented in the context of the FEniCS finite element software. We illustrate the new features through a range of examples, including a constrained Poisson problem, a set of Stokes-type flow models and a model for ionic electrodiffusion.

CCS Concepts: • **Mathematics of computing** → **Solvers**; **Partial differential equations**; • **Computing methodologies** → *Modeling methodologies*.

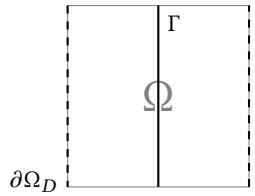
Additional Key Words and Phrases: FEniCS project, mixed dimensional, mixed domains, mixed finite elements

1 INTRODUCTION

Mixed dimensional partial differential equations (PDEs) are systems of differential equations coupling solution fields defined over domains of different topological dimensions. Problem settings that call for such equations are in abundance across the natural sciences [27, 47], in multi-physics problems [13, 48], and in mathematics [8, 29]. For instance, in geology, fluid flow through faults and fractures in rocks can be modelled via mixed dimensional PDEs posed on a hierarchy of interacting domains of heterogeneous dimension [9, 44]. In physiology, such equations can model blood flow in a three-dimensional lumen interacting with a topologically two-dimensional elastic membrane i.e. the vessel wall [13]. Generally, Lagrange multipliers on lower-dimensional spaces are commonly used to impose non-standard boundary conditions or continuity properties over interfaces between subdomains [7, 47], see e.g. Figure 1 below for an idealized example.

For the numerical solution of mixed dimensional PDEs, the finite element method is a natural approach [10, 15, 19]. However, the efficient implementation of finite element discretizations for mixed dimensional PDEs is non-trivial – for a number of reasons. First, such discretizations involve manipulations of multiple meshes and submeshes of heterogeneous topological dimension. Second, the computation of local (element-wise) finite element tensors involve integrals of possibly restrictions of basis functions defined on cells of different dimensions. Third, the global assembly of the finite element matrices involve local-to-global mappings across different meshes and submeshes. And finally, the solution of the resulting linear systems require efficient and appropriate linear algebra structures. As a result, the widespread application of mixed dimensional PDEs by domain

Authors' addresses: Cécile Daversin-Catty, Simula Research Laboratory, P.O. Box 134, 1325, Lysaker, Norway, cecile@simula.no; Chris N. Richardson, BP Institute, University of Cambridge, Madingley Road, Cambridge, CB3 0EZ, United Kingdom, cnr12@cam.ac.uk; Ada J. Ellingsrud, Simula Research Laboratory, P.O. Box 134, 1325, Lysaker, Norway, ada@simula.no; Marie E. Rognes, Simula Research Laboratory, P.O. Box 134, 1325, Lysaker, Norway, meg@simula.no.



$$-\Delta u = f \quad \text{on } \Omega, \tag{1a}$$
$$u = c \quad \text{on } \Gamma, \tag{1b}$$
$$u = 0 \quad \text{on } \partial\Omega_D, \tag{1c}$$
$$\frac{\partial u}{\partial n} = 0 \quad \text{on } \partial\Omega \backslash \partial\Omega_D. \tag{1d}$$

Fig. 1. Find the solution $u : \Omega \to \mathbb{R}$ to the Poisson equation (1) with mixed homogeneous boundary conditions on a two-dimensional unit square $\Omega = [0, 1] \times [0, 1] \subset \mathbb{R}^2$ such that u is a constant c along the topologically one-dimensional interior surface $\Gamma = \{(x, y) \,|\, x = 0.5, y \in (0, 1)\}$. To satisfy the latter constraint, introduce a Lagrange multiplier $\lambda : \Gamma \to \mathbb{R}$.

specialists is hindered by a lack of numerical solution techniques and easy-to-use yet efficient software tools.

In view of the wide range of applications for mixed dimensional PDEs, a number of finite element software packages implement some mixed domain and mixed dimensional finite element features, including `FreeFem++` [21], `Feel++` [38], `deal.II` [6], or `PorePy` [26]. In particular, `FreeFem++` [21] handles Lagrange multipliers in mixed and mortar methods defining finite element spaces on boundary meshes. `deal.II` [6] supports Lagrange multipliers on embedded, possibly non-matching, meshes, and in particular implements immersed finite elements methods [22]. `Feel++` [38] also handles mixed-dimensional problems defining trace meshes, used for example when implementing domain decomposition and mortar methods [42]. Finally, `PorePy` [26] implements mixed dimensional geometrical features providing an explicit representation of fractures with both finite volumes and virtual finite element discretizations. Still, the combination of a generic, automated and high-level software interface would allow for more rapid development of mixed dimensional discretizations and more widespread use.

Over the last 15 years, there has been a significant and growing interest in generic, high-performance finite element frameworks, as demonstrated by e.g. the FEniCS Project [1, 20, 31], the Firedrake Project [39], Feel++ [38], FreeFEM [21] and NGSolve [43]. A shared design pattern is the combination of a high-level specification of the problem discretization, lower-level algorithms for problem solution, and automated code generation to bridge the gap between. This approach has been extremely successful, allowing for rapid development of advanced efficient numerical solvers for non-trivial PDEs and deployment by application scientists. In particular, FEniCS is organized as an open source collection of software components including the high-level domain-specific Unified Form Language (UFL) [2], the FEniCS Form Compiler (FFC) [32], and the problem solving environment DOLFIN [33, 34]. We refer to the above references for a more in-depth description of the FEniCS approach and components.

While FEniCS has offered native support for immersed manifolds since 2012 [41], support for discretizations of mixed domain- and mixed dimensional PDEs has been lacking in the core library. In response and driven by extensive user demand, several FEniCS extensions have been developed to remedy the situation. For instance, `fenics_ii` [23] implements the concept of trace spaces, while the `multiphenics` Python library [5] provides tools aiming to ease the prototyping of multiphysics problems. However, we argue that native support for mixed dimensional finite element methods within the core FEniCS framework is advantageous as it allows for e.g. increased robustness in part due to more extensive testing and wider distribution, and easier development of auxiliary packages and techniques such as e.g. the automated derivation of adjoint models [20]. Moreover, a

formal description of the abstractions and algorithms involved in finite element methods for mixed dimensional PDEs is needed.

This work addresses and resolves the gap in available abstractions and algorithms, and importantly the formal description of such, for the automated numerical solution of mixed dimensional PDEs via finite element methods. In particular, we propose and advocate a light-weight design pattern for mixed dimensional finite element abstractions. We revise and introduce new abstractions in the Unified Form Language for mixed function spaces, basis functions and integration domains allowing for coupled variational formulations defined over mixed domains. We also introduce a generalized assembly algorithm together with associated features such as submesh generation and block matrices. For the automated generation of local element tensor code from the symbolic representation, i.e. the form compilation, we present form component extraction algorithms and revised form compilation strategies.

The concepts and algorithms presented here are implemented in UFL [2], FFC [32] and DOLFIN [33], and are openly and freely available (see [16, 17]). The scope of this paper is limited to mixed domain and mixed dimensional problems of co-dimension one at most, i.e. nD-mD problems with $|n-m| \leqslant 1$ and to conforming meshes. Various techniques for handling non-matching meshes are discussed in the literature, such as e.g [12, 24], but not considered further here.

This paper is organized as follows. In Section 2 we describe the mathematical scope of our mixed domain and mixed dimensional framework. We then address different aspects of the finite element method applied to mixed domain problems including key challenges in the subsequent sections. Section 3 is dedicated to meshes, nested submeshes and mappings between such. The key features in UFL for defining and manipulating mixed domain function spaces and variational forms are introduced in Section 4. The local-to-global degree of freedom mapping is introduced in Section 5 as a key ingredient for the assembly of mixed domain and mixed dimensional variational forms. Abstract assembly algorithms, building on the construction of local element tensors and subsequent insertion using the local-to-global degree of freedom mappings, are detailed in Section 6. An overview of the revised FEniCS user interface and pipeline is given in Section 7 with emphasis on automated code generation of mixed domain and mixed dimensional local tensors and assembly features. Importantly, we present numerical results for various applications in Section 8 ranging from the an idealized reference example introduced as Example 1 to more advanced models highlighting the relevance of our framework in biomedical applications. Section 9 provides some concluding remarks while discussing current limitations and future extensions.

2 MATHEMATICAL SCOPE AND CONCEPTS

2.1 Notation

For convenience, we here provide an overview of the main notation used in this manuscript. In general, superscripts are used to indicate subdomain or block indices. In the text, all indices start at 1. In the code, the corresponding indices start at 0. The terms element and element-wise are used equivalently with cell or cell-wise, respectively.

i, j: Indices associated with the number of subdomains.
n, m: Indices associated with number of basis functions.
r, s: Indices associated with form arity.
$|S|$: Dimension of a finite set S.
Ω, Ω^i: A domain, domain i for $i = 1, \ldots, I$.
d^i: Topological dimension of Ω^i.
$\mathbb{V}^i$: Vector space relative to Ω^i.
$\mathcal{T}, \mathcal{T}^i$: A simplicial mesh, simplicial mesh of Ω^i.

$\mathcal{S}(\mathcal{T})$: The simplicial complex induced by the simplicial mesh $\mathcal{T}$.
U^i: Finite element function space defined with respect to $\mathcal{T}^i$.
N^i: Dimension of the finite element space U^i: $N^i = \dim(U^i)$.
N^i_K: Dimension of the finite element space U^i restricted to K: $N^i_K = \dim(U^i|_K)$. If K is a cell in $\mathcal{T}^i$, this is the local dimension of the finite element space U^i.
ϕ^i_n: Basis function for U^i for $n = 1, \dots, N^i$.
$\mathcal{N}^i_K$: A set of indices of basis functions in U^i with K in their support: $\mathcal{N}^i_K = \{n \in \{1, \dots, N^i\} \mid K \subseteq \text{supp}(\phi^i_n)\}$.
$\mathcal{V}, \mathcal{V}^i$: Set of n_v, n^i_v vertex indices in $\mathcal{T}, \mathcal{T}^i$.
$\mathcal{F}, \mathcal{F}^i$: Set of n_f, n^i_f facet indices in $\mathcal{T}, \mathcal{T}^i$.
$\mathcal{C}, \mathcal{C}^i$: Set of n_c, n^i_c cell indices in $\mathcal{T}, \mathcal{T}^i$.
$\mathcal{M}^i_v, \mathcal{M}^i$: Child-to-parent vertex and cell index maps.
ι^i_K: Local-to-global degree of freedom map, $K \in \mathcal{T}^i$, for finite element space U^i.
S_K: Star of K, defined as the set of cells in $\mathcal{T}$ containing K.

2.2 Mixed domains and meshes

We define a mixed domain PDE as a system of PDEs coupling fields $u^i : \Omega^i \to \mathbb{V}^i$ where $\Omega^i \subset \mathbb{R}^d$ is a bounded domain of geometrical dimension d and topological dimension d^i, and $\mathbb{V}^i$ is a vector space for $i = 1, \dots, I$. We assume that there exists an $\Omega \subset \mathbb{R}^d$, a d-dimensional domain that embeds all the subdomains $\Omega^i \subseteq \Omega$, with $d \geqslant \max_i d^i$. We refer to Ω as the parent domain. We assume that Ω is polyhedral such that it admits a conforming discretization. The subdomains are assumed to be of codimension at most one relative to Ω, i.e. $|d^j - d^i| \leqslant 1$ for all $i, j = 1, \dots, I$. We will use the term mixed dimensional PDE for a mixed domain PDE if there are i, j such that $d^i \neq d^j$.

We assume that the parent domain Ω is partitioned by a mesh $\mathcal{T}$ consisting of a finite set of cells $\mathcal{T} = \{K\}$. For simplicity in terminology, we here consider the case of simplicial cells (intervals, triangles, tetrahedra). Moreover, we assume that we can define a conforming mesh $\mathcal{T}^i$ of each subdomain Ω^i, for $i = 1, \dots, I$, consisting of mesh entities (vertices, edges, faces, cells) from $\mathcal{T}$. More precisely, we assume that $\Omega^i = \cup_k \{K^i_k\}$ where the submesh $\mathcal{T}^i = \{K^i_k\}_k$ consists of mesh entities K^i_k from $\mathcal{T}$. In the language of complexes, let $S(\mathcal{T})$ be the simplicial complex defined by $\mathcal{T}$. By definition, Ω is then the underlying space of S. We assume that $\mathcal{T}$ and Ω^i for $i = 1, \dots, I$ are such that we can define simplicial meshes $\mathcal{T}^i$ with induced simplicial complexes $\mathcal{S}^i = \mathcal{S}(\mathcal{T}^i)$ such that Ω^i is the underlying space of $\mathcal{S}^i$ and such that $\mathcal{S}^i$ is a subcomplex of $\mathcal{S}$ for $i = 1, \dots, I$.

2.3 Finite element function spaces

We introduce function spaces U^i for $i = 1, \dots, I$, each defined over Ω^i, such that

$$U^i = \{v^i : \Omega^i \to \mathbb{V}^i\}, \tag{2}$$

and assume that each unknown $u^i \in U^i$. The solution u of a mixed domain PDE is hence an I-tuple $u = (u^1, \dots, u^I)$ in the Cartesian product space U:

$$u \in U \equiv U^1 \times U^2 \times \cdots \times U^I. \tag{3}$$

We refer to U as a mixed function space with U^i as subspaces.

We are here mainly concerned with finite element spaces U^i defined relative to the submeshes $\mathcal{T}^i$ for $i = 1, \dots, I$. We assume that these discrete function spaces are indeed finite element spaces in the sense that the basis functions have localized support and can be defined element-wise. We write N^i for the global dimension of the finite element space U^i, and N^i_K for its local (element-wise) dimension i.e. $\dim(U^i|_K)$ for $K \in \mathcal{T}^i$. We denote by $\{\phi^i_n\}_{n=1}^{N^i}$ the sets of basis functions spanning

the discrete spaces U^i. Discrete solutions $u^i \in U^i$, for $i = 1, \ldots, I$, can thus be expressed as a linear combination of these basis functions:

$$u^i = \sum_{n=1}^{N^i} \bar{u}_n^i \phi_n^i, \tag{4}$$

with expansion coefficients (or, colloquially, degrees of freedom) $\bar{u}_n^i$ for $n = 1, \ldots, N^i$. We emphasize the possibility of having different kinds of finite element spaces for the different function spaces. This is especially relevant for multiphysics problems for which the suitable function space properties can differ from one field to the other.

2.4 Variational forms and formulations

We consider discrete variational formulations of systems of linear or non-linear PDEs and associated variational forms of arity $r \geq 0$. For time-dependent problems, we presuppose a time-stepping procedure yielding systems of PDEs at each time step. In general, we consider systems of PDEs that may be expressed in operator form with $I \in \mathbb{N}$ equations, each defined over Ω^i for $i = 1, \ldots, I$. As our main emphasis is on finite element discretizations, we assume that a discrete variational formulation of the system is prescribed.

2.4.1 Linear variational problems. We first consider a general system of discrete linear variational equations: find $u \in U = U^1 \times U^2 \times \cdots \times U^I$ such that

$$a^i(u, v^i) = L^i(v^i) \quad \forall\, v^i \in U^i \quad i = 1, \ldots, I, \tag{5}$$

where $a^i : U \times U^i \to \mathbb{R}$ is a bilinear form, $L^i : U^i \to \mathbb{R}$ is a linear form, and U^i are appropriate finite element spaces defined over Ω^i and mapping into $\mathbb{V}^i$, for $i = 1, \ldots, I$. To enhance readability, note that we present the case of coinciding trial and test subspaces here, however we include numerical examples with differing test and trial spaces in Section 8.

By the linearity of a^i and as the approximation space U is defined as a Cartesian product of function spaces cf. (3), each bilinear form a^i can be written as the sum of bilinear forms $a^{i,j} : U^j \times U^i \to \mathbb{R}$:

$$\exists\, a^{i,j} \mid a^i(u, v^i) = \sum_{j=1}^{I} a^{i,j}(u^j, v^i) \quad \forall\, i = 1, \ldots, I. \tag{6}$$

The discrete weak form of the whole coupled system for linear mixed problems thus consists in finding $u \in U$ such that

$$a(u, v) = L(v) \qquad \forall\, v \in U, \tag{7}$$

with $v = (v^1, \ldots, v^I)$ and

$$a(u, v) = \sum_{i=1}^{I} \sum_{j=1}^{I} a^{i,j}(u^j, v^i) \quad \text{and} \quad L(v) = \sum_{i=1}^{I} L^i(v^i). \tag{8}$$

In general, a variational form $a : U \times U \times \cdots \times U$ of arity r can be decomposed into r sums of arity-r forms: $a^{i_1, i_2, \ldots, i_r} : U^{i_r} \times U^{i_{r-1}} \times \cdots \times U^{i_1} :\to \mathbb{R}$:

$$a(u_r, u_{r-1}, \ldots, u_1) = \sum_{i_1=1}^{I} \cdots \sum_{i_r=1}^{I} a^{i_1, i_2, \ldots, i_r}(u_r^{i_r}, u_{r-1}^{i_{r-1}}, \ldots, u_1^{i_1}). \tag{9}$$

for $u_s = (u_s^1, u_s^2, \ldots, u_s^I)$ for $s = 1, \ldots, r$. We will refer to $a^{i_1, i_2, \ldots, i_r}$ and specifically $a^{i,j}$ and L^i as block forms. We will refer to a (block) form $a^{i_s, i_s, \ldots, i_s}$ for some $s \in \{1, \ldots, r\}$ as a diagonal (block) form.

The finite element solution of (7) typically involves the assembly of the bilinear form a and linear form L, i.e. the construction of a matrix A and a vector L such that u solves

$$A\bar{u} = b, \tag{10}$$

where $\bar{u}$ denotes the vector of expansion coefficients for the discrete field u i.e.

$$\bar{u} = \{\bar{u}^i\}_{i=1}^I, \quad \bar{u}^i = \{\bar{u}^i_n\}_{n=1}^{N^i} \quad \forall\, i = 1, \dots, I. \tag{11}$$

By construction, cf. (8), A is a block matrix and b is a block vector with entries

$$\left[\begin{array}{c|c|c} A^{1,1} & \dots & A^{1,I} \\ \hline \vdots & \ddots & \vdots \\ \hline A^{I,1} & \dots & A^{I,I} \end{array}\right] \left[\begin{array}{c} \bar{u}^1 \\ \hline \vdots \\ \hline \bar{u}^I \end{array}\right] = \left[\begin{array}{c} b^1 \\ \hline \vdots \\ \hline b^I \end{array}\right]. \tag{12}$$

The diagonal blocks $A^{i,i}$ represent the uncoupled parts of the problem while the off-diagonal blocks $A^{i,j}$ for $i \neq j$ represent the interaction between fields living on any two subdomains Ω^i and Ω^j. The elements of A and b are defined for $i, j = 1, \dots, I$ by

$$A^{i,j}_{m,n} = a^{i,j}(\phi^j_n, \phi^i_m) \text{ and } b^i_m = L^i(\phi^i_m),\ n = 1, \dots, N^j,\ m = 1, \dots, N^i. \tag{13}$$

Example 1. *To illustrate, we detail a variational formulation and the block structure of the mixed dimensional Poisson example introduced in Figure 1. As detailed in Section 2.2, we assume a mesh $\mathcal{T}$ of the parent domain Ω such that a subset of its facets induce a conforming submesh $\mathcal{T}^2$ of Γ. We identify $\Omega^1 = \Omega$, $\mathcal{T}^1 = \mathcal{T}$ and $\Omega^2 = \Gamma$. Further, we let $U^1 \subset H^1_0(\Omega^1)$ be a finite element space with zero trace on the Dirichlet boundary $\partial\Omega_D$ only, and let U^2 be a conforming finite element space of $L^2(\Omega^2)$. A discrete variational formulation describing (1) then reads: find $(u, \lambda) \in U \equiv U^1 \times U^2$ such that*

$$\int_\Omega \nabla u \cdot \nabla v \,\mathrm{d}x + \int_\Gamma \lambda v \,\mathrm{d}s + \int_\Gamma \eta u \,\mathrm{d}s = \int_\Omega f v \,\mathrm{d}x + \int_\Gamma c\eta \,\mathrm{d}s, \tag{14}$$

for all $(v, \eta) \in U^1 \times U^2$.

The block decomposition (8) of the bilinear form $a(u, v)$ (resp. linear form $L(v)$) gives the subforms

$$a^{1,1}(u, v) = \int_\Omega \nabla u \cdot \nabla v \,\mathrm{d}x, \quad a^{1,2}(\lambda, v) = \int_\Gamma \lambda v \,\mathrm{d}s, \quad a^{2,1}(u, \eta) = \int_\Gamma \eta u \,\mathrm{d}s,$$

with $a^{2,2}(\lambda, \eta) = 0$, and

$$L^1(v) = \int_\Omega f v \,\mathrm{d}x, \quad L^2(\eta) = \int_\Gamma c\eta \,\mathrm{d}s.$$

The block system corresponding to (14) then reads as follows (with $u = u^1$ and $u^2 = \lambda$):

$$\left[\begin{array}{c|c} A^{1,1} & A^{1,2} \\ \hline A^{2,1} & A^{2,2} \end{array}\right] \left[\begin{array}{c} \bar{u}^1 \\ \hline \bar{u}^2 \end{array}\right] = \left[\begin{array}{c} b^1 \\ \hline b^2 \end{array}\right], \tag{15}$$

where the blocks $A^{i,j}$ and b^i, $i, j = 1, 2$ are obtained from (13).

2.4.2 Nonlinear variational problems. Nonlinear mixed domain problems lead to discrete variational formulations of the form: find $u \in U$ such that

$$F^i(u; v^i) = 0 \quad \forall\, v^i \in U^i, \tag{16}$$

where the forms $F^i : U \times U^i \to \mathbb{R}$ may be nonlinear in $u \in U$ but are linear in the test functions $v^i \in U^i$ for $i = 1, \ldots, I$. Combining the I equations, the canonical nonlinear mixed formulation reads as: find $u \in U$ such that

$$F(u; v) = 0 \quad \forall\, v \in U, \tag{17}$$

with

$$F(u; v) = \sum_{i=1}^{I} F^i(u; v^i). \tag{18}$$

Newton's method or variations are commonly used to solve such problems. Starting from an initial solution $u_0 = (u_0^1, \ldots, u_0^I)$, each iteration solves the system

$$J(u_k; \cdot, v)(u_{k+1} - u_k) = -F(u_k; v), \tag{19}$$

where $J(u_k; \cdot, v)$ is the Jacobian of $F(u_k; v)$ at the k-th iteration. The discrete system at each iterate again has a block-shaped pattern

$$\left[\begin{array}{c|c|c} J^{1,1} & \ldots & J^{1,I} \\ \hline \vdots & \ddots & \vdots \\ \hline J^{I,1} & \ldots & J^{I,I} \end{array}\right] \left[\begin{array}{c} \delta u^0 \\ \hline \vdots \\ \hline \delta u^I \end{array}\right] = - \left[\begin{array}{c} F^1 \\ \hline \vdots \\ \hline F^I \end{array}\right], \tag{20}$$

and $u_{k+1} = u_k + \delta u$, with blocks defined by:

$$J^{i,j}_{m,n} = \frac{\partial F^i(u_k; \phi^i_m)}{\partial u^j}\left(\phi^j_n\right) \text{ and } F^i_m = F^i(u_k; \phi^i_m), \tag{21}$$

for $n = 1, \ldots, N^j$, $m = 1, \ldots, N^i$ and $i, j = 1, \ldots, I$.

2.5 Integration domains

Typically in finite element applications, the mixed variational forms, e.g. a and L in (7) and F in (17), are given as sums of integrals over different subdomains Ω^i. We assume that all variational forms can be represented by sums over mesh entities, for instance as sums of integrals over cells in a domain, see e.g. [31]. For mixed dimensional problems, the subdomains Ω^i will have different topological dimensions $d^i \leqslant d$, where d is the topological dimension of the parent domain Ω. We introduce the notation $x = (x_1, \ldots, x_d)$ for the coordinates of a point $x \in \Omega$. In the following, the notation $\mathrm{d}x = \mathrm{d}x_1 \times \cdots \times \mathrm{d}x_d$ is used in integrals over a d-dimensional domain. We use the notation $\mathrm{d}s$ to integrate over a co-dimension 1 subdomain of Ω.

The implementation of finite element discretizations of mixed domain problems within a high level framework such as e.g. the FEniCS Project involves a number of new concepts and algorithmic extensions in comparison with single domain problems. We dive into these aspects in the subsequent sections.

3 DATA STRUCTURES FOR NESTED SUBMESHES

In this section, we discuss and suggest data structures for representing submeshes, in particular for nested submeshes. As detailed in Section 2.2, we consider the case where all subdomains Ω^i share a parent domain Ω and where each subdomain is covered by a conforming submesh $\mathcal{T}^i$ of the parent complex generated by $\mathcal{T}$. Two mappings between meshes are essential for mixed domain finite element assembly: first, mappings between submesh entities and parent mesh entities, and second, mappings between mesh entities in different submeshes. In the below, we formalize these concepts and describe their implementation in the FEniCS context.

3.1 Mappings for nested submeshes

We assume that each mesh is represented by the combination of its topology (defining the mesh entities and connections between these) and geometry (defining the spatial vertex coordinates) [30]. We denote by n_v, n_f and n_c the number of vertices, facets and cells in $\mathcal{T}$, respectively, and let $\mathcal{V}$, $\mathcal{F}$ and $\mathcal{C}$ be the corresponding sets of vertex, facet and cell indices:

$$\mathcal{V} = \{v_k\}_{k=1}^{n_v},\ \mathcal{F} = \{f_k\}_{k=1}^{n_f} \text{ and } \mathcal{C} = \{c_k\}_{k=1}^{n_c}. \tag{22}$$

We assume that any vertex, facet and cell can be identified by the respective index v_k, f_k and c_k and its (mesh entity) type. For each submesh, we denote by $\mathcal{V}^i$ and $\mathcal{C}^i$ the sets of vertex and cell indices of $\mathcal{T}^i$, whose indices v_k^i and c_k^i are independent from the parent mesh numbering cf. (22):

$$\mathcal{V}^i = \{v_k^i\}_{k=1}^{n_v^i},\ \mathcal{C}^i = \{c_k^i\}_{k=1}^{n_c^i}. \tag{23}$$

We now introduce two maps that link the vertex indices in the submesh with the corresponding vertex index in the parent mesh, and the cell indices in the submesh with the corresponding mesh entity index in the parent mesh. In particular, for each submesh $\mathcal{T}^i$, we define its (child-to-parent) vertex map $\mathcal{M}_v^i$ and cell map $\mathcal{M}^i$:

$$\mathcal{M}_v^i : \mathcal{V}^i \to \mathcal{V} \quad \text{and} \quad \mathcal{M}^i : \mathcal{C}^i \to \mathcal{E} \in \{\mathcal{C}, \mathcal{F}\}. \tag{24}$$

We note that if the submesh $\mathcal{T}^i$ has the same topological dimension as its parent $\mathcal{T}$, each cell in the submesh is a cell in the parent mesh and so $\mathcal{E} = \mathcal{C}$. However, the cells of a submesh of codimension $e \geq 1$ are mesh entities of codimension e in the parent mesh $\mathcal{T}$, and $\mathcal{E} = \mathcal{F}$ when $e = 1$. These concepts applied to the reference example (1) are illustrated in Figure 2.

A mixed domain problem can couple an arbitrary but finite number I of fields $u^i \in \Omega^i$, $i = 1, \ldots, I$. The assembly of the systems (12), (20) can then require additional mappings $\mathcal{M}^{i,j}$ to relate the submeshes $\mathcal{T}^i$ and $\mathcal{T}^j$ involved in e.g. $a^{i,j}$ (8) for $i \neq j$ as illustrated by Figure 3, assuming their intersection $\mathcal{T}^i \cap \mathcal{T}^j$ is non-empty. Assume that $d^j \geq d^i$ without further loss of generality. We can then express the map from cell indices of $\mathcal{T}^i \in \mathcal{T}^i \cap \mathcal{T}^j$ to corresponding mesh entity indices in $\mathcal{T}^j$ as

$$\mathcal{M}^{i,j} : \mathcal{C}^i \to \mathcal{E}^j, \quad \mathcal{E}^j \in \{\mathcal{F}^j, \mathcal{C}^j\}. \tag{25}$$

As all submeshes $\mathcal{T}^i$, $i = 1, \ldots, I$ share the same parent mesh $\mathcal{T}$ by assumption, we can use the mappings $\mathcal{M}^i$ and $\mathcal{M}^j$ (24) to establish the relation between $\mathcal{C}^i$ and $\mathcal{C}^j$. If $\mathcal{T}^i$ and $\mathcal{T}^j$ have the same topological dimension ($d^i = d^j$), then the cell map between the two submeshes can be expressed directly as

$$\mathcal{M}^{i,j} = \left(\mathcal{M}^j\right)^{-1} \circ \mathcal{M}^i : \mathcal{C}^i \longrightarrow \mathcal{C}^j. \tag{26}$$

On the other hand, if $d^i \neq d^j$ i.e. $d^i = d^j - 1$, then the computation of $\mathcal{M}^{i,j}$ requires additional intermediate steps. The mapping $\mathcal{M}^i : \mathcal{C}^i \to \mathcal{F}$ (24) gives the facet index $f_k \in \mathcal{T}$ associated with the lower dimensional cell index $c_k \in \mathcal{T}^i$. The mesh connectivity, relating entities of various dimension within the same mesh, denoted as $(d-1) \to d$ in [30], gives the indices of the (two) cells

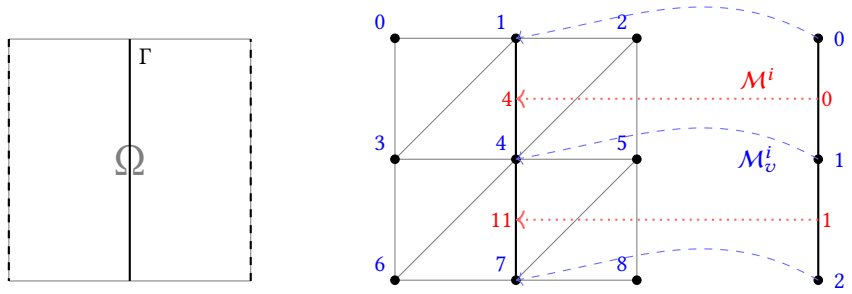


Fig. 2. Mapping between a submesh and its parent. The parent mesh $\mathcal{T}$ is the 2D mesh representing Ω, while the submesh $\mathcal{T}^1$ represents the interface Γ and can be constructed as a subset of $\mathcal{T}$ facets. The parent mesh has $n_v = 9$ vertices ($\mathcal{V} = \{0, \ldots, 8\}$) and $n_f = 16$ facets ($\mathcal{F} = \{0, \ldots, 15\}$), while the submesh $\mathcal{T}^1$ has $n^1_v = 3$ vertices ($\mathcal{V}^1 = \{0, 1, 2\}$) and $n^1_c = 2$ cells ($\mathcal{C}^1 = \{0, 1\}$). The mappings $\mathcal{M}^1_v : \mathcal{V}^1 \to \mathcal{V}$ and $\mathcal{M}^1 : \mathcal{C}^1 \to \mathcal{F}$ cf. (24) give $\mathcal{M}^1_v(0) = 1$, $\mathcal{M}^1_v(1) = 4$, $\mathcal{M}^1_v(2) = 7$ and $\mathcal{M}^1(0) = 4$, $\mathcal{M}^1(1) = 11$.

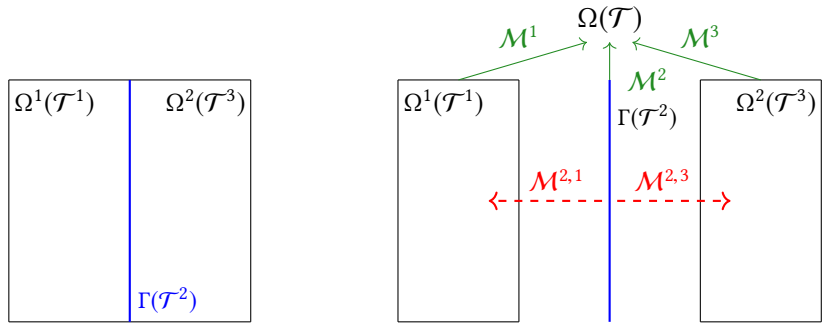


Fig. 3. The assembly of the systems can require additional mappings $\mathcal{M}^{i,j}$ to relate the submeshes $\mathcal{T}^i$ and $\mathcal{T}^j$ with $i \neq j$, assuming they are built from the same parent $\mathcal{T}$. For example, the additional mapping $\mathcal{M}^{2,1}$: $\mathcal{C}^2 \to \mathcal{F}^1$ is needed and only built if $a^{1,2}(\phi^2_n, \phi^1_m)$ or $a^{2,1}(\phi^1_m, \phi^2_n)$ is non-zero, $n = 1, \ldots, N^2$, $m = 1, \ldots, N^1$.

adjacent to f_k in $\mathcal{T}$. The inverse mapping $\left(\mathcal{M}^j\right)^{-1} : \mathcal{C} \to \mathcal{C}^j$ gives their equivalent indices in the submesh $\mathcal{T}^j$. Finally, the facet $f \in \mathcal{F}^j$ shared by these cells can be found via the mesh connectivity $d^j \to (d^j - 1)$ in $\mathcal{T}^j$. The mapping $\mathcal{M}^{i,j} : \mathcal{C}^i \longrightarrow \mathcal{F}^j$ (27) is then obtained:

$$\mathcal{C}^i \xrightarrow{\mathcal{M}^i} \mathcal{F} \xrightarrow{(d-1)\to d} \{\mathcal{C}, \mathcal{C}\} \xrightarrow{\left(\mathcal{M}^j\right)^{-1}\times 2} \{\mathcal{C}^j, \mathcal{C}^j\} \xrightarrow{d^j \to (d^j-1)} \mathcal{F}^j \tag{27}$$

3.2 Nested submesh algorithms in FEniCS

In this section, we discuss algorithms for nested submeshes and associated parent-child relationships in the context of the FEniCS/DOLFIN finite element library.

The DOLFIN `Mesh` class provides data structures and algorithms for computational meshes holding the underlying geometry and topology through dedicated objects `MeshGeometry` and `MeshTopology` [30, 33]. The `MeshGeometry` stores the coordinates of the mesh vertices, while the `MeshTopology` defines the mesh entities (vertices, edges, facets and cells) and their connections. The mesh entities are labeled by pairs $e = (d, e_j)$ defining each entity e from its index e_j within the set of entities of topological dimension d. To represent discrete functions defined over mesh entities, for instance a map from cell indices to specific integer values, DOLFIN provides the class(es) `MeshFunction`.

To efficiently represent meshes for mixed domain discretizations, we introduce a new lightweight `MeshView` class. This class is designed to allow for representing and building submeshes $\mathcal{T}^i$ as new `Mesh` objects while storing their relationship with the parent mesh $\mathcal{T}$. A `MeshView` object links two meshes (for instance a submesh and its parent mesh, or two submeshes) by holding pointers to the parent (or associated) mesh $\mathcal{T}$ together with the vertex and cells maps $\mathcal{M}_v^i$ and $\mathcal{M}^i$. Further, we let the `MeshTopology` of a (sub)mesh hold a map of `MeshViews` with the identifier of the parent (or associated) meshes as keys. To reduce complexity, we consider one generation of meshes: i.e. we only support parent-child and sibling meshes.

To construct a submesh, we assume that a `MeshFunction` defined over the parent mesh encodes the selected subset of mesh entities by an integer, referred to as a tag. The `MeshView` class implements a `create` function which builds the submesh $\mathcal{T}^i$ and its child-to-parent maps $\mathcal{M}_v^i$ and $\mathcal{M}^i$ (24) from this `MeshFunction` and the corresponding tag. This function returns a new `Mesh` object, with a pointer to the `MeshView` object in its `MeshTopology`, and its use is illustrated in Listing 1.

```
# Define function over facets in parent mesh to represent tags
marker = MeshFunction("size_t", mesh, 1, 0)
for f in facets(mesh):
  marker[f] = 0.5 - eps < f.midpoint().x() < 0.5 + eps
# Build the submesh T^2 from the facets marked as 1
submesh = MeshView.create(marker, 1)
```

Listing 1. [Python] Creation of the submesh $\mathcal{T}^2$ from the parent mesh $\mathcal{T}$ (see Figure 2 and Figure 3) for Example 1 using the `MeshView` class.

In addition to mapping between mesh entities of a submesh and its parent, mixed domain form assembly typically requires knowledge of mesh entity mappings between different submeshes as illustrated by Figure 3. We also represent these mappings via the `MeshView` class, and provide a new `build_mapping` function to construct these maps. In particular, for submeshes $\mathcal{T}^i$ and $\mathcal{T}^j$ with a shared parent mesh $\mathcal{T}$, `build_mapping` creates a new `MeshView` object pointing to the associated mesh $\mathcal{T}^j$, a cell map defined by (26) and an empty vertex map by default. This `MeshView` is then added to the map of `MeshViews` associated with the `MeshTopology` of submesh $\mathcal{T}^i$, in addition to its initial parent mesh view. Mappings between submeshes are built (and stored) on-the-fly during mixed domain form assembly as illustrated in Listing 2. In particular, we do not build unnecessary mappings $\mathcal{M}^{i,j} : \mathcal{C}^i \to \mathcal{E}^j$.

```
// List of a^{i,j} integration mesh mappings (MeshView map)
auto mesh_mapping = _a[i][j]->mesh()->topology().mapping();
// Add mapping with TestFunction mesh if needed
auto mesh0 = _a[i][j]->function_space(0)->mesh();
if(_a[i][j]->mesh() != mesh0 && !mesh_mapping.count(mesh0->id()))
  _a[i][j]->mesh()->build_mapping(mesh0);
```

Listing 2. [C++] Illustration of additional mappings between submeshes being built on-the-fly during form assembly. For each subform $a^{i,j}$ (`_a[i][j]`), `build_mapping` is called to build the mapping between the integration mesh (`_a[i][j]->mesh()`) and each basis function mesh (`mesh0`) unless it exists i.e. unless the mapping is already listed in the `MeshTopology` of the integration mesh.

3.3 Algorithmic complexity of submesh algorithms

The algorithmic complexity of the submesh construction can be estimated as follows. The construction of each submesh $\mathcal{T}^i$ requires iterating over the n_c^i marked entities in the parent $\mathcal{T}$. The mapping $\mathcal{M}^i$ (24) is then obtained and can be stored directly. The storage of the n_v^i vertices of

$\mathcal{T}^i$ to build the underlying `MeshGeometry` and the mapping $\mathcal{M}_v^i$ (24) requires iterating over the local vertices of each cell c in the submesh $\mathcal{T}^i$, representing a complexity of $O(n_v^i)$. The `MeshTopology` holds the previously built mappings $\mathcal{M}^i$ and $\mathcal{M}_v^i$ and the numbering of $\mathcal{T}^i$ entities obtained directly by an iterative loop over both mappings whose complexity is $O(n_v^i + n_c^i)$. In parallel, the `MeshTopology` also requires the global numbering within the scope of the parallel computation communicator. Since $\mathcal{M}^i$ and $\mathcal{M}_v^i$ are locally built on each processor, the global numbering needs additional loops and parallel communications to establish the ownership of the shared entities. Each additional mapping (26) requires iterating over the n_c^i cells of $\mathcal{T}^i$ to find their counterparts in $\mathcal{T}^j$, $i \neq j$, hence representing a $O(n_c^i)$ complexity. Taking all into account, the submesh construction scales with the size of the mesh, and is a scalable parallel algorithm.

3.4 MPI-parallelism of nested submeshes and mappings

DOLFIN [31] is designed to be seamlessly parallel, meaning that the same code can be used to perform both serial and parallel simulations. On distributed memory architectures, the parallel support relies on the Message Passing Interface (MPI). DOLFIN automatically performs mesh partitioning in parallel using the libraries ParMETIS [25] or SCOTCH [37]. Each processor holds only a portion of the global mesh, stored as a standard `Mesh` object, for which it is responsible. Data exchange between processors then requires the computation of local-to-global[1] maps on each process. The nested submeshes $\mathcal{T}^i$ are assumed to be built from a common parent mesh $\mathcal{T}$. When running a mixed-dimensional simulation in parallel, the partitioning of the submeshes stems from the partitioning of the parent mesh $\mathcal{T}$, i.e. no auxiliary partitioning is performed. Thus, it is possible for a submesh to be distributed over only some of the available processors. And vice versa, it may be that a processor does not own any entities of a given submesh.

As described in Section 3.2, the submeshes $\mathcal{T}^i$ are represented as standard `Mesh` objects storing a `MeshView` in their `MeshTopology`. As for the global mesh $\mathcal{T}$, the submeshes $\mathcal{T}^i$ require a local-to-global mapping to communicate data between processors, which implies establishing the ownership of each submesh entity among the processors. We assume that the cells can belong to only one partition, i.e. we do not introduce ghost cells. Each cell c_k^i in C^i is owned by the processor owning the corresponding entity $\mathcal{M}^i(c_k^i)$ in $\mathcal{T}$. However, the vertices located at the interface between partitions are shared by a set of processors. Among these, the vertices are assumed to be owned by the processor with the lowest rank. This processor holds the underlying local-to-global mapping and sends it to the other processors involved. Thus, a cell owned by a processor of rank i may have vertices owned by a processor of rank j, where $j < i$.

4 FORM LANGUAGE ABSTRACTIONS AND ALGORITHMS FOR MIXED DOMAINS

The Unified Form Language (UFL) [1, 2] is a domain-specific language for finite element spaces, tensor algebra and variational forms. It provides a flexible interface for defining variational formulations of differential equations, through abstractions closely mimicking the mathematical syntax. UFL includes a set of predefined base finite element families, including but not limited to Lagrange [10], Discontinuous Galerkin [3], Raviart–Thomas [40], Brezzi-Douglas-Marini [11], Nédelec [35, 36], of arbitrary polynomial dimension. The UFL finite element definition mimics that of Ciarlet [14], and in particular, a finite element is defined relative to a reference element (and not to a mesh). Mixed finite elements can be defined as Cartesian products of the base element families, assuming that all subelements share a common reference cell. A UFL function space is defined by a pairing of a (mixed) finite element and a domain (representing e.g. the mesh). However, for mixed domain and dimensional problems, these abstractions are not sufficient.

[1] In this section local-to-global refers to process-to-communicator (local to process, global to communicator).

To extend UFL with abstractions for mixed domain variational problems, we advocate a lightweight approach, essentially representing mixed function spaces (in contrast to function spaces over mixed elements) as tuples of function spaces. This design choice mirrors our design choice for finite element assembly of mixed domain variational forms using block tensors. We detail the new UFL abstractions for mixed (domain) function spaces and integration in Sections 4.1 and 4.2 below. To facilitate mixed domain assembly, we have also extended UFL with new algorithms for splitting mixed domain variational forms into sums of subforms, described in Section 4.3. Finally, we describe UFL form validation and typical non-admissible operations in Section 4.4.

4.1 Mixed function spaces and functions

To represent a mixed domain discrete function space $U = U^1 \times \cdots \times U^I$ composed of a finite number I of finite element function spaces U^i for $i = 1, \ldots, I$, we introduce a new[2] UFL class `MixedFunctionSpace`. This lightweight class simply holds a tuple of the component spaces $(U^1, \ldots, U^I)$, and sample usage is provided in Listing 3. The key operational aspect of the `MixedFunctionSpace` abstraction is the identification of the relative position of a subfunction space and argument within the product space.

```
# U = U^1 x U^2
U1 = FunctionSpace(mesh, "CG", 2)
U2 = FunctionSpace(submesh, "DG", 1)
U = MixedFunctionSpace(U1, U2)
```

Listing 3. [Python] Example of `MixedFunctionSpace` usage in UFL/DOLFIN to define a mixed function space with two component spaces defined relative to different meshes.

UFL distinguishes between two types of functions appearing in variational forms: (i) `Argument`s representing the basis functions for a function space and (ii) `Coefficients` representing any function in a function space, i.e. a weighted linear combination of basis functions. A `TrialFunction` and `TestFunction` represent pre-indexed `Arguments` with index corresponding to the order of the argument in the form(s). UFL assumes that a variational form is always linear in its `Arguments` but possibly nonlinear in its `Coefficients`. To define test and trial functions on a mixed function space, and arguments in general, the syntax `TestFunctions`, `TrialFunctions` and `Arguments` have been adopted. This syntax is illustrated in Listing 4 below. These operators, when acting on a `MixedFunctionSpace` with I subspaces, return a tuple of basis functions u^i for $i = 1, \ldots, I$, as a list of `Argument` objects embedding the block index i of the underlying function spaces U^i.

```
(u0, [...], uI) = TrialFunctions(U) # u = (u^1,...,u^I)
(v0, [...], vI) = TestFunctions(U)  # v = (v^1,...,v^I)
(w0, [...], wI) = Arguments(U)      # w = (w^1,...,w^I)
(f0, [...], fI) = Coefficients(U)   # f = (f^1,...,f^I)
```

Listing 4. [Python] Basis functions (`Arguments`, and more specifically `TestFunctions` and `TrialFunctions`), or any functions (`Coefficients`) of a `MixedFunctionSpace` are defined as a list of functions embedding the block index of the underlying function space.

[2]The keyword `MixedFunctionSpace` existed in previous versions of UFL, but was deprecated in version 2016.1.0. It has now been reintroduced in a more generic context handling mixed domain and mixed dimensional function spaces.

4.2 Measures for mixed domain variational forms

In UFL [2], integrals are expressed through multiplication ($*$) by a measure representing the integral type. The main integral types are: `dx` for integrals over the interior of the domain, `ds` for the exterior facets i.e. the integrals over the boundary, and `dS` for the set of interior facets. Integrals over different parts of the domain can be expressed using markers given as an optional parameter `subdomain_data` and specifying the corresponding tag in the form expression. The terminal operands involved in the form integrals are `Arguments` and `Coefficients`, carrying their associated function space(s) and thereby the associated mesh(es) (see Listing 4). When the form arguments belong to the same function space i.e. for monodomain problems or for diagonal block forms, only one mesh is involved and the integration domain can thus be deduced without explicit definition by the measure.

For off-diagonal block forms, involving function spaces defined over different submeshes, the integration domain must be explicitly specified by measure (re)definition. Typical usage is illustrated in Listing 5.

```
dx1 = Measure("dx", domain=U1.mesh()) # Integral over Ω¹
dx2 = Measure("dx", domain=U2.mesh(), subdomain_data=...) # Ω²
ds1 = Measure("ds", domain=U1.mesh()) # ∂Ω¹
```

Listing 5. [Python] Example of redefining measures to define the integration domain of a form integral, giving explicitly the integral type, the integration mesh and possibly a marker to handle integrals over different parts of the domain.

When a measure is used in a form (integral), we assume that the measure's domain and the function space mesh of at least one of the form arguments coincide. Further, the redefined measures should define integration over cells for a lower dimensional mesh rather than integration over facets for a higher dimensional mesh.

With the measures defined in Listing 5, we can express the variational formulation of the Poisson problem introduced in Example 1 as follows (Listing 6).

```
a = inner(grad(u),grad(v))*dx1 + v*l*dx2(1) + u*e*dx2(1)
```

Listing 6. [Python] UFL/DOLFIN implementation of the variational form (14) from Example 1 with explicit specification of the integration domains.

4.3 Mixed domain variational form algorithms

A key advantage of UFL and similar domain specific languages is the ability to manipulate e.g. variational forms at the symbolic level. In the context of mixed domain variational forms, a key operation is to extract subform blocks i.e. to compute a decomposition into subforms (such as e.g. (8)) of a mixed domain form. For instance, to assemble mixed domain variational forms, we advocate a block-by-block approach for the sake of flexibility, efficiency and reuse. This is also the approach considered by [5, 23]. For automated block-by-block assembly, the automated extraction of subforms from a variational form defined over a mixed function space is convenient.

To extract the subforms $a^{i,j}$ from a bilinear form a (and the analogous for linear forms), we have introduced a UFL function `extract_blocks`. Its underlying algorithm relies on the directed acyclic graph (DAG) representation used by UFL [2, 31] to represent the form integrands. For any given bilinear form a, its DAG expression tree allows the identification and extraction of the terms involving the pair (U^j, U^i) of subspaces as the subform $a^{i,j}$, given the corresponding indexing $i, j = 1, \ldots, I$. This algorithm relies on the embedding of the block index with the `MixedFunctionSpace`. The function `extract_blocks` can either return the whole list of subforms of a

given form, or a specific subform $a^{i,j}$ given the indices (i, j). A code example demonstrating the usage of this function is presented in Listing 7 below.

```
# a(u,v) = ∑_i ∑_j a^{i,j}(u^j, v^i)
a = u0*v0*dx0 + ... ui*vj*dxi + ... + uI*vI*dxI
# as ≡ [a^{0,0},...,a^{i,j},a^{i,j+1},...,a^{i+1,j}...,a^{I,I}]
as = extract_blocks(a)
# a_ij ≡ a^{i,j}(u^j, v^i)
a_ij = extract_blocks(a,i,j)
```

Listing 7. [Python] The `extract_blocks` function is used to extract the subforms $a^{i,j}$ of the mixed domains form $a(u, v) = \sum_i \sum_j a^{i,j}(u^j, v^i)$ from the arguments indexing. The subform $a^{1,2}$ from Example 1 implemented as in Listing 6 can be obtained using `a_12 = extract_blocks(a,0,1)`. Note again that the indices start at 0 in the code.

4.4 UFL mixed domain form verification

The following code checks have been introduced to prevent confusion or misuse of the mixed domain features. All UFL verification assertions for single domain variational forms have been extended to mixed domain forms by application to each block subform.

Regarding the mixed function spaces definition, a `MixedFunctionSpace` is not a `FunctionSpace`, but rather a list of `FunctionSpace` objects. Arguments (resp. coefficients/functions) defined from a `MixedFunctionSpace` form a list of `Arguments` (resp. `Coefficients`) corresponding to each block. Thus, only the plural version of the related keywords are allowed: `TrialFunction(V)` is not allowed when `V` is a `MixedFunctionSpace`. Instead, `TrialFunctions(V)` should be used.

The coupling of arguments and/or functions from different function spaces in a form requires the underlying objects to be defined from a `MixedFunctionSpace`. In other words, combining `TrialFunction(V1)` and `TestFunction(V2)` with `V1` and `V2` defined as different `FunctionSpaces` is not supported. One should instead introduce `V` as a `MixedFunctionSpace(V1,V2)` and define the arguments (`TestFunctions(V)` and `TrialFunctions(V)`) from the latter.

The assembly of off-diagonal blocks combining arguments from different function spaces requires a mapping between the (sub)meshes involved, as discussed in Section 3. To define this mapping, we assume that the submeshes share a common parent mesh. This assertion is checked at the mesh data structure level, e.g. when building mappings between the submeshes within the `build_mapping` function. Finally, a form integral is not valid if the integration mesh defined through the integral's measure does not coincide with one of the meshes associated with the form arguments.

5 MIXED DOMAIN FUNCTION SPACES AND DEGREES OF FREEDOM

In this section, we discuss the transfer of local-to-global degree-of-freedom maps between submeshes. These maps are used in mixed domain assembly algorithms, described in detail in Section 6.

Consider a mesh $\mathcal{T}^i = \{K\}$ and a finite element space U^i defined relative to $\mathcal{T}^i$. The standard local-to-global mapping $\iota^i_{c^i}$ for the finite element space U^i and a cell $K \in \mathcal{T}^i$ with cell index $c^i \in \mathcal{C}^i$ maps the set of local basis function indices to the corresponding global indices:

$$\iota^i_{c^i} : \{1, \dots, N^i_K\} \to \{1, \dots N^i\}, \tag{28}$$

where N^i denotes the (global) dimension of U^i and N^i_K denotes the (local) dimension of $U^i|_K$ for each K, see e.g. [31] for more details. We assume that the local-to-global map $\iota^i_{c^i}$ is available for each submesh $\mathcal{T}^i$.

First, consider the case of two submeshes $\mathcal{T}^1$ and $\mathcal{T}^2$ with a parent mesh $\mathcal{T}$ with $d = d^1 = d^2$ as illustrated in Figure 4. Consider two function spaces $U^1 = U^1(\mathcal{T}^1)$ and $U^2 = U^2(\mathcal{T}^2)$. For each $K \in \mathcal{T}^1$ (resp. $K \in \mathcal{T}^2$) with index $c^1 \in \mathcal{C}^1$ (resp. $c^2 \in \mathcal{C}^2$), we can use the mapping $\mathcal{M}^1$ (resp. $\mathcal{M}^2$) to access the cell index c relative to the parent mesh $\mathcal{T}$:

$$c = \mathcal{M}^1(c^1) = \mathcal{M}^2(c^2). \tag{29}$$

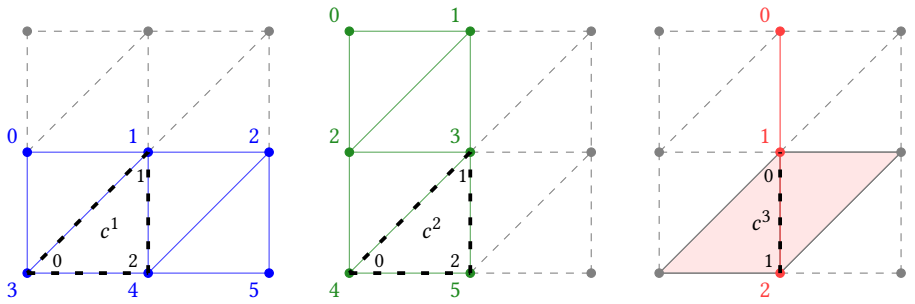
When there is a coupling between $\mathcal{T}^1$ and $\mathcal{T}^2$, the mapping $\mathcal{M}^{2,1}$ can be used to get the cell index $c^1 \in \mathcal{C}^1$ of K relative to $\mathcal{T}^1$ from its index $c^2 \in \mathcal{C}^2$ relative to $\mathcal{T}^2$:

$$c^1 = \mathcal{M}^{2,1}(c^2). \tag{30}$$

Subsequently, we can define the global index n for the local (degree-of-freedom) index l for K in U^i via

$$n = \iota^i_{c^i}(l), \tag{31}$$

for $l = 1, \ldots, N^i_K$.



(a) K in $\mathcal{T}^1$ (b) K in $\mathcal{T}^2$ (c) K in $\mathcal{T}^3$

Fig. 4. Illustration of submesh mappings and local-to-global degrees of freedom numbering. (a) The submesh $\mathcal{T}^1$ defined as the lower half of $\mathcal{T}$ with global degrees of freedom numbering (in blue) of $U^1(\mathcal{T}^1)$. The cell K with index $c^1 \in \mathcal{C}^1$ has $N^1_K = 3$ local degrees of freedom. The local-to-global relationship (31) gives $\iota^i_{c^1}(0) = 3$, $\iota^i_{c^1}(1) = 1$ and $\iota^i_{c^1}(2) = 4$. (b) The submesh $\mathcal{T}^2$ defined as the left half of $\mathcal{T}$ with global degrees of freedom numbering (in green) of $U^2(\mathcal{T}^2)$. The cell K with index $c^2 \in \mathcal{C}^2$ has $N^2_K = 3$ local degrees of freedom (in black) with $\iota^i_{c^2}(0) = 4$, $\iota^i_{c^2}(1) = 3$ and $\iota^i_{c^2}(2) = 5$. (c) The lower-dimensional submesh $\mathcal{T}^3$ defined as the middle vertical line of $\mathcal{T}$ with global degrees of freedom numbering (in red) of $U^3(\mathcal{T}^3)$. The cell K with index $c^3 \in \mathcal{C}^3$ has $N^3_K = 2$ local degrees of freedom (in black) with $\iota^i_{c^3}(0) = 1$ and $\iota^i_{c^3}(1) = 2$. The star S_K of K is composed of two cells (in light red).

Next, consider the case of two submeshes $\mathcal{T}^1$ and $\mathcal{T}^3$ with a parent mesh $\mathcal{T}$ with $d = d^1 > d^3$ and a function space U^1 defined relative to $\mathcal{T}^1$. For each $K \in \mathcal{T}^3$, we define its star S_K as the set of cells in $\mathcal{T}$ containing K (see Figure 4c). Take $\tilde{K} \in S_K$ and let $c \in \mathcal{C}$ be its cell index relative to $\mathcal{T}$. By stipulation, $\tilde{K}$ is also a cell in $\mathcal{T}^1$, but its cell index c^1 relative to $\mathcal{T}^1$ is given by

$$c^1 = (\mathcal{M}^1)^{-1}(c).$$

This relation can thus be used to transfer local-to-global maps of degrees of freedom.

6 MIXED DOMAIN FINITE ELEMENT ASSEMBLY

The finite element assembly of a variational form a of arity r is the computation of the r-tensor A resulting from evaluating the variational form over its range of basis functions. A variational form can consist of multiple integrals, each with its own integration domain. A typical finite element assembly algorithm iterates over the cells K of each integration domain $\mathcal{K}$ to compute the global finite element tensor A by (i) evaluating local (cell-wise) element tensors A^K and (ii) inserting (or adding) these into the global tensor via a local-to-global degree-of-freedom mapping. For more details on finite element assembly in general, see e.g. [31].

6.1 Mixed domain assembly challenges and discussion of approach

In single domain finite element assembly, the basis functions and coefficients are defined on one mesh $\mathcal{T}$ and the integration domains are defined relative to this mesh. For the assembly of mixed domain variational forms, we here consider a block-by-block approach as illustrated by e.g. the decomposition (8) and the resulting block linear system (12) for bilinear forms and the general (9). In particular, we assemble each integral of each block form separately. Diagonal block forms are defined relative to a single domain, and can thus be assembled using standard single domain assembly algorithms. We therefore do not discuss these further here, but rather focus on the off-diagonal blocks. These present a number of additional challenges:

- Assembly of off-diagonal blocks requires knowledge of the relationships between the integration mesh given by the form measure and the meshes involved in the trial and test spaces. These relationships are obtained through mappings between the parent-child or sibling meshes as discussed in Section 3.
- New techniques are required for the evaluation (and form compilation) of local element tensors over function spaces defined over different domains and dimensions.

In single domain finite element assembly, each local element tensor corresponds to the contribution from a single element. In mixed dimensional finite element assembly, the finite element tensor can again be formed by combining local element tensor contributions. However, the local element tensor concept is more multifaceted. Below, we introduce two local tensor concepts for mixed dimensional variational forms: the composite local element tensor and the local element tensor.

6.2 Mixed domain assembly of cell integrals

We analyze the assembly of a mixed domain variational block form of arity r in further detail, using a bilinear form ($r = 2$) as a guiding case. The discussion is analogous for general r-forms. Consider an off-diagonal block form $a^{i,j} : U^j \times U^i \to \mathbb{R}$ for a fixed $i \neq j$ and assume without loss of generality that $\Omega^i \cap \Omega^j \neq \emptyset$, but that $\Omega^i \neq \Omega^j$. To alleviate notation, we just write $a = a^{i,j}$, and set $i = 1$ and $j = 2$, again without loss of generality. We further assume that a represents a single integral, cf. Section 2.5, noting that sums of integrals are easily handled. Thus, we have that

$$a : U^2 \times U^1 \to \mathbb{R}, \quad a(\cdot, \cdot) = \sum_{K \in \mathcal{K}} a^K(\cdot, \cdot), \tag{32}$$

where $\mathcal{K}$ is the integration domain of dimension $d^{\mathcal{K}}$, assumed to be (a subset of) the cells in either $\mathcal{T}^1$ or $\mathcal{T}^2$ (cf. Section 4.2). Specifically, we need to evaluate

$$A^K_{m,n} = a^K(\phi^2_n, \phi^1_m), \tag{33}$$

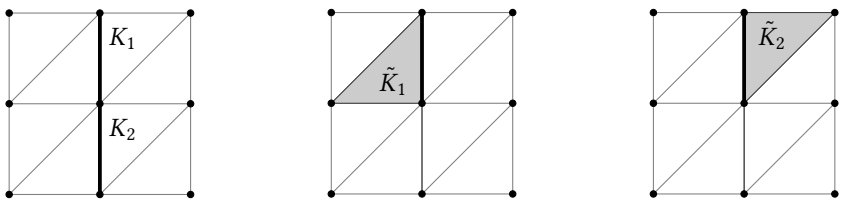
for all $m = 1, \ldots, N^1$, $n = 1, \ldots, N^2$.

6.2.1 Case 1 (homogeneous dimension) $d^{\mathcal{K}} = d^1 = d^2$. If Ω^1 and Ω^2 both have the topological dimension of the integration mesh $d^{\mathcal{K}} = d^1 = d^2 \leq d$, the finite element spaces U^1 and U^2 can be defined over the same reference cell. In this case, the assembly of the local tensors A^K (33) can be handled by standard techniques. However, the insertion into the global tensor A requires knowledge of the global degree of freedom numberings n^1 and n^2 relative to U^1 and U^2, respectively. These indices are obtained through the local-to-global mappings (31) as illustrated in Algorithm 1.

Algorithm 1 Assembly of bilinear cell integrals over homogeneous dimensions

```
for K in 𝒦 do
    Compute the cell indices c¹ and c² of K relative to 𝒯¹ and 𝒯², respectively
    Compute A_K
    for l₁ ← 1, ..., N¹_K and l₂ ← 1, ..., N²_K do
        Compute m = ι¹_{c¹}(l₁) and n = ι²_{c²}(l₂)
        Add entry (l₁, l₂) of A_K to A at entry (m, n)
    end for
end for
```

6.2.2 Case 2 (codimension one) $d^{\mathcal{K}} = d^2 = d^1 - 1$. Assume that U^1 and U^2 have different topological dimensions with $d^1 > d^2$, and more specifically that $d^1 = d^2 + 1$. The set $\mathcal{K}$ in (32) must then be (a subset of) the cells in $\mathcal{T}^2$ and (a subset of) the facets in $\mathcal{T}^1$. Each cell in $\mathcal{K}$ is either an interior facet in $\mathcal{T}^1$, in which case it is shared between two cells, or an exterior facet, in which case it belongs to a single cell and is located on the boundary of $\mathcal{T}^1$. We focus on the case of interior facets. The case of exterior facets is analogous but simpler. For instance, if $\mathcal{T}$ is a two-dimensional mesh of triangles, $\mathcal{T}^1$ is a (sub)mesh of triangles, and $\mathcal{T}^2$ is a (topologically one-dimensional) submesh of intervals, then $\mathcal{K}$ must be a subset of the intervals in $\mathcal{T}^2$. This setting is illustrated for Example 1 in Figure 5.



(a) $\mathcal{K} = \{K_1, K_2\}$ in $\mathcal{T}^2$ (b) $\tilde{K}_1 \subset S_K$ in $\mathcal{T}^1$ (c) $\tilde{K}_2 \subset S_K$ in $\mathcal{T}^1$

Fig. 5. Mesh entities involved in the local element tensors of mixed dimensional terms for bilinear forms. To exemplify, we consider a parent mesh $\mathcal{T}$ of dimension $d = 2$ and a continuous piecewise linear finite element space U^1 defined over a mesh $\mathcal{T}^1 = \mathcal{T}$ of topological dimension $d^1 = 2$ and a continuous piecewise linear finite element space U^2 defined over a mesh $\mathcal{T}^2$ of topological dimension $d^2 = 1$. (a) Let $\mathcal{K} = \{K_1, K_2\} \subset \mathcal{T}^2$ be the integration domain. (b)-(c) For each $K \in \mathcal{K}$, we define its star $S_K = \{\tilde{K}_1, \tilde{K}_2\} \subset \mathcal{T}^1$ as the (two) adjoining cells in $\mathcal{T}^1$ each with K as a facet.

Consider an element $K \in \mathcal{K}$. We note that $a^K(\phi_n^2, \phi_m^1)$ will be zero for all $m = 1, \ldots, N^1$, $n = 1, \ldots, N^2$ for which $\phi_m^1|_K = 0$ or $\phi_n^2|_K = 0$. Conversely, $a^K(\phi_n^2, \phi_m^1)$ is potentially non-zero if K is in the support of both ϕ_m^1 and ϕ_n^2 i.e. $K \subset \text{supp}(\phi_m^1) \cap \text{supp}(\phi_n^2)$. We denote the set of U^i basis function indices with K in their support by $\mathcal{N}_K^i$ i.e. $\mathcal{N}_K^i = \{n \in \{1, \ldots, N^i\} | K \subseteq \text{supp}(\phi_n^i)\}$. Thus, potentially $a_K(\phi_n^2, \phi_m^1) \neq 0$ for $m \in \mathcal{N}_K^1$ and $n \in \mathcal{N}_K^2$, and $a_K(\phi_n^2, \phi_m^1) = 0$ otherwise. Since

$K \in \mathcal{T}^2$, the number of U^2 basis functions with K in their support equals the local (cell) dimension of U^2: $N_K^2 = \dim(\mathcal{N}_K^2) = \dim(U^2|_K)$. On the other hand, for K viewed as an interior facet in $\mathcal{T}^1$, we define its star $S_K = \{\tilde{K}_1, \tilde{K}_2\}$ as the set of the (two) cells in $\mathcal{T}^1$ with K as a facet (see Figure 5). The number of U^1 basis functions with K in their support equals the dimension of U^1 restricted to the star: $N_{S_K}^1 = \dim(\mathcal{N}_K^1) = \dim(U^1|_{S_K})$. For exterior facets, we simply define the star as the single cell with K as a facet.

To proceed, we introduce two new local tensor concepts for mixed dimensional variational forms. We define the *composite local element tensor* $A_{q,l}^K$ as the (potentially) non-zero contributions from the cell $K \in \mathcal{K} \subseteq \mathcal{T}^2$ to the global tensor:

$$A_{\kappa,l}^K = a^K(\phi_n^2, \phi_m^1), \quad m = \iota_{\tilde{c}}^1(\kappa), n = \iota_{c^2}^2(l), \quad \kappa = 1, \dots, N_{S_K}^1, l = 1, \dots, N_K^2. \tag{34}$$

where $\iota_{\tilde{c}}^i$ is a map from (local) degree-of-freedom indices of cells $\tilde{K} \subset S_K$ with index $\tilde{c}$ to global degree-of-freedom indices for U^i (here for $i = 1$). Subsidiary, for each $K \in \mathcal{K}$ and for each $\tilde{K} \in S_K$, we define the *local element tensor* $A_{k,l}^{\tilde{K},K}$ as

$$A_{k,l}^{\tilde{K},K} = a^K(\phi_n^2, \phi_m^1), \quad m = \iota_{c^1}^1(k), n = \iota_{c^2}^2(l), \quad k = 1, \dots, N_{\tilde{K}}^1, l = 1, \dots, N_K^2. \tag{35}$$

for any $\tilde{K} \in \mathcal{T}^1$ with index c^1 and $K \in \mathcal{K} \subseteq \mathcal{T}^2$ with index c^2. We note that $m = \iota_{c^1}^1(k)$ can be computed via the submesh mapping transfer of the local-to-global mapping as described in Section 5. Since $K \in \mathcal{T}^2$, the local-to-global mapping $\iota_{c^2}^2$ is immediately available. The composite local element tensor can be expressed in terms of the local element tensors as

$$A_{\kappa,l}^K = A_{k,l}^{\tilde{K},K}, \quad \kappa = \gamma^1(k), k = 1, \dots, N_{\tilde{K}}^1, l = 1, \dots, N_K^2, \quad \tilde{K} \in S_K. \tag{36}$$

where $\kappa = \gamma^1(k)$ is an appropriate map of local basis function indices on $\tilde{K}$ to composite local basis function indices on S_K. However, we note that the composite local element tensor A^K need not be formed explicitly; rather selected parts of the local element tensors $A^{K,\tilde{K}}$ for $\tilde{K} \in S_K$ can be added directly to the global tensor.

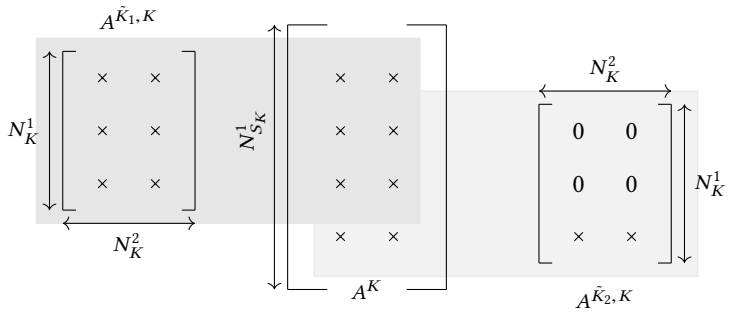


Fig. 6. Non-zero contributions to the element tensors for mixed dimensional (bilinear) forms cf. Example 1 and Figure 5. The composite local element tensor A^K, corresponding to the potentially non-zero entries of A^K for $K \in \mathcal{K} \subseteq \mathcal{T}^2$ can be defined by selecting contributions from $\tilde{K}_1$ and $\tilde{K}_2$. N_K^i is the local (element-wise) dimension of U^i for $i = 1, 2$. The entries of the local tensor $A^{\tilde{K}_2,K}$ that have already been accounted for though $A^{\tilde{K}_1,K}$ can be zeroed in order to avoid adding a contribution twice.

To avoid counting the same contribution twice when directly adding the local local tensors $A^{\tilde{K},K}$ to the global tensor A, the following approach may be used. If the star is composed of two cells $S_K = \{\tilde{K}_1, \tilde{K}_2\}$ as shown in Figure 5, the local tensor $A^{\tilde{K}_2,K}$ contains entries that have already been

added to the global tensor when adding $A^{\tilde{K}_1,K}$. In particular, the entries $A^{\tilde{K}_2,K}_{k_2,l}$, $l = 1,\dots,N^2_K$ may be replaced by zero when it exists a $k_1 \in \{1,\dots N^1_{\tilde{K}_1}\}$ such that $\gamma^1(k_2) = \gamma^1(k_1)$ (see Figure 6).

Example 2. *To illustrate the above ideas and concepts, we consider the computation of the finite element tensors for Example 1. We let U^1 and U^2 be finite element spaces of continuous piecewise linears defined relative to $\mathcal{T}^1$ and $\mathcal{T}^2$, respectively, and consider the off-diagonal matrix block $A^{1,2}$ corresponding to the form $a^{1,2}$ for each cell $K \in \mathcal{T}^2$ (corresponding to interior facets in $\mathcal{T}^1$):*

$$a^{K,1,2}(\phi^2_n, \phi^1_m) = \int_K \phi^2_n \phi^1_m \,\mathrm{d}x, \quad \forall\, m \in N^1, n \in N^2. \tag{37}$$

Again, for readability, we drop the superscript $\cdot^{1,2}$ in the following. The composite local element tensors of a can be computed by selecting contributions from the elements of the star S_K, as illustrated in in Figure 5 and Figure 6. For this specific set of U^1 and U^2, $\dim(\mathcal{N}^1_K) = 4$ and $\dim(\mathcal{N}^2_K) = 2$.

In conclusion, a standard cell-wise finite element assembly algorithm can be augmented by an additional inner loop over adjacent mesh entities (stars) to allow for assembly of mixed dimensional cell integrals. The algorithm is given in Algorithm 2.

Algorithm 2 Assembly of bilinear cell integrals over mixed dimensions

```
for K in 𝒦 (with cell index c² relative to 𝒯² ≡ 𝒦) do
    for K̃ in S_K do
        Compute the cell index c¹ of K̃ relative to 𝒯¹
        Compute A_{K,K̃}
        for l₁ ← 1,...,N¹_K and l₂ ← 1,...,N²_K do
            Compute m = ι¹_{c¹}(l₁) and n = ι²_{c²}(l₂)
            Zero previously computed rows A^{K̃,K}
            Add entry (l₁, l₂) of A^{K̃,K} to A at entry (m, n)
        end for
    end for
end for
```

Finally, the case where U^1 and U^2 have the same topological dimensions $d^1 = d^2$, but the integration domain is of lower dimension $d^{\mathcal{K}} < d^1 = d^2$ can be viewed as an extension of the previous Case 2 where the star $S_K = \{\tilde{K}_1, \tilde{K}_2\}$ is handled as $S_K = S^1_K \cup S^2_K$ where $S^1_K = \{\tilde{K}_1\}$ (resp. $S^2_K = \{\tilde{K}_2\}$) is the star relative to $\mathcal{T}^1$ (resp. $\mathcal{T}^2$). We do not discuss this case further here.

Remark 1 (Assembly of facet and vertex integrals). *The dedicated algorithms presented here for mixed dimensional assembly focus on cell integrals, assuming other integral types to be defined as cell integrals over a lower-dimensional mesh. Standard assembly algorithms may handle various other integral types, e.g. facet or point assembly. We remark that these other types of integrals can be used as usual for diagonal blocks as the latter rely only on single domain assembly algorithms.*

Remark 2 (Mixed dimensional assembly with higher dimensional gaps). *In general, and in particular for submeshes with codimension more than one, the star S_K may contain an arbitrary number of cells in $\mathcal{T}$ sharing the lower dimensional cell K. We emphasize that the algorithms we have presented to form the composite local tensors A^K can be applied to stars S_K with an arbitrary number of elements. In particular, this design easily allows for extensions to higher dimensional gaps, e.g. assembly of coupled 3D-1D variational forms.*

7 OVERVIEW OF NEW FENICS USER INTERFACE AND PIPELINE

The abstractions and algorithms presented in this paper have been implemented in the FEniCS finite element framework [1]. Both low level and high level features are available in C++ and Python. Use of the high level interface for solving mixed dimensional variational problems is exemplified in Listing 8, which solves the reference Poisson problem introduced in Section 1 (Example 1).

```
from dolfin import *

# Generate the meshes
mesh = UnitSquareMesh(n, n)
marker = MeshFunction("size_t",mesh,mesh.topology().dim()-1,0)
for f in facets(mesh):
    marker[f] = 0.5 - EPS < f.midpoint().x() < 0.5 + EPS
submesh = MeshView.create(marker,1)

# Initialize function spaces and basis functions
V = FunctionSpace(mesh, "CG", 1)
LM = FunctionSpace(submesh, "CG", 1)
W = MixedFunctionSpace(V,LM)
(u,l) = TrialFunctions(W)
(v,e) = TestFunctions(W)

# Dirichlet boundary condition(x = 0 or x = 1)
def boundary(x):
    return x[0] < DOLFIN_EPS or x[0] > 1.0 - DOLFIN_EPS
bc = DirichletBC(V, Constant(0.0), boundary)

# Variational formulation
dV = Measure("dx", domain=W.sub_space(0).mesh())
dL = Measure("dx", domain=W.sub_space(1).mesh())
a = inner(grad(u),grad(v))*dV + v*l*dL + u*e*dL
L = Constant(2)*v*dV + Constant(0.25)*e*dL

# Solve the problem
sol = Function(W)
solve(a == L, sol, bc)
```

Listing 8. [Python] Illustration of mixed dimensional functionalities usage to solve the reference Poisson problem introduced as Example 1. The dedicated abstractions easily integrate the language, keeping the code syntax close to the mathematical formulation.

The `solve` function in the last line of Listing 8 encapsulates the whole mixed domains problem solving process including the extraction of block forms (see Section 4), the compilation and code generation for each resulting subform, the block-by-block assembly (see Section 6), and the solving of the recombined block system using a given solver. The presented framework covers a wide range of applications, and for the sake of flexibility, intermediate lower-level functions are also available. For instance, access to and manipulation of the separate matrix blocks can be used for preconditioning and iterative solution purposes. The overall structure of the mixed domain functionality is illustrated in Figure 7, while more implementation details are presented in the next sections.

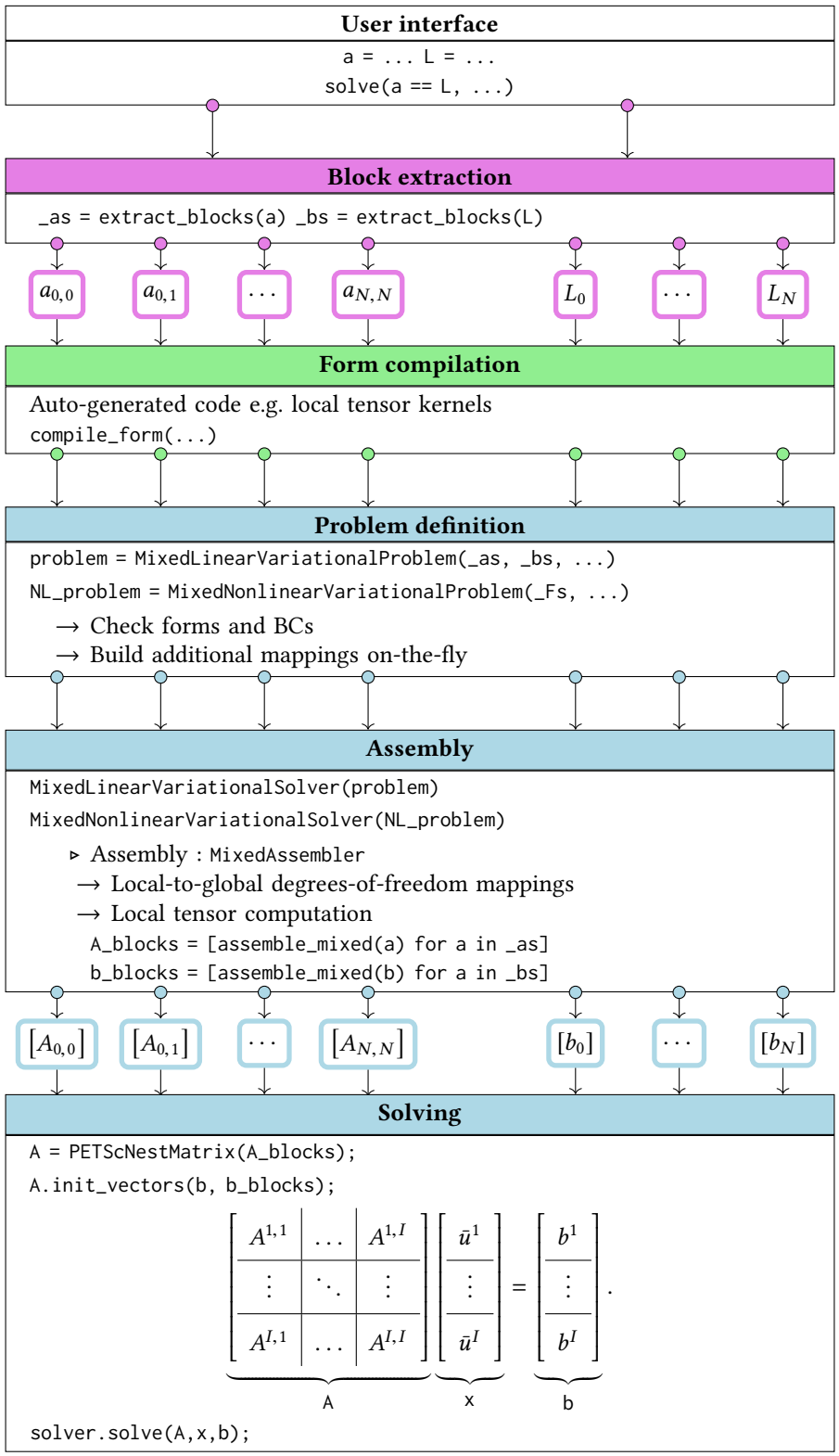


Fig. 7. Overview of the FEniCS user interface for mixed dimensional problems. The block colors refer to the FEniCS component impacted : •:UFL •:FFC •:DOLFIN

7.1 Code generation of local tensors for mixed dimensional forms

The code for computing of the local tensors A^K (`tabulate_tensor`) together with related quantities required for the assembly is auto-generated by the form compiler FFC [32] given a variational form. Hence, each variational form has its own kernel implementing the computation of the corresponding local tensors A^K depending on the finite element, the integration domain and the form itself. In particular, the measures `dx`, `ds` and `dS` discussed in Section 4.2 to represent the different integral types (cell integral, integral over exterior facets and over interior facets, respectively) are mapped to different implementations of the `tabulate_tensor` function with appropriate signatures.

The `tabulate_tensor` relative to cell integrals, shown in Listing 9 below, takes as argument the local tensor `A` to be computed, together with information about the cell geometry, the coordinates of its degrees of freedom and the form coefficients if any.

```
void tabulate_tensor(double * A,
                     const double * const * w,
                     const double * coordinate_dofs,
                     int cell_orientation)
```

Listing 9. [C++] Signature of the `tabulate_tensor` function dedicated to local tensor computation of cell integrals.

The computation of the local tensors for exterior facet integrals requires the local index of the corresponding facet in the cell as an additional argument, cf. Listing 10.

```
void tabulate_tensor(double * A,
                     const double * const * w,
                     const double * coordinate_dofs,
                     std::size_t facet,
                     int cell_orientation)
```

Listing 10. [C++] Signature of the `tabulate_tensor` function dedicated to local tensor computation of exterior facet integrals.

The algorithms presented in this paper focus on cell assembly, assuming that measures in mixed-dimensional forms define integration over cells of the lower dimensional mesh. The cell assembly of mixed forms with homogeneous dimension involves a single reference cell whose local tensors A^K are computed as usual using Listing 9. On the other hand, the codimension one local tensors $A^{\tilde{K},K}$, relative to the cells $\tilde{K}$ in the star S_K, can be assembled as exterior facet integrals over the lower dimensional cell K. To accommodate for such computations, the `tabulate_tensor` signature for cell integrals has been revised, see Listing 11. In particular, we have added an optional input argument `local_facet` to mimic the `facet` argument of Listing 10.

```
void tabulate_tensor(double * A,
                     const double * const * w,
                     const double * coordinate_dofs,
                     int cell_orientation,
                     std::size_t local_facet = 0)
```

Listing 11. [C++] Signature of the revised `tabulate_tensor` function dedicated to local tensor computation of cell integrals for handling codimension one local tensors.

7.2 FEniCS interface to mixed domains assembly

The FEniCS assembler implementation has been revised to tackle mixed domain assembly of cell integrals as described in Section 6. We present the revised assembly algorithms for the case of homogeneous dimension (but mixed domains) and heterogeneous dimension (mixed dimensional) in the respective sections below.

The insertion of the local tensors A^K and $A^{\tilde{K},K}$ into the block tensor requires the local-to-global degree of freedom mappings discussed in Section 5. The cell indices c^i relative to $\mathcal{T}^i$ required for the mappings $\iota^i_{c^i}$ (28) are stored in a double-indexed array `cell_index[i][j]`. The first index `i` represents the submesh $\mathcal{T}^i$, `i=0` (resp. `i=1`) corresponding to the test (resp. trial) function space. The second index `j` denotes the `j`-th contribution $\tilde{K}$ of S_K in the case of heterogeneous dimension. These cell indices are obtained from the parent-child and sibling mesh mappings introduced in Section 3.

7.2.1 Case 1 (homogeneous dimension) $d^{\mathcal{K}} = d^1 = d^2$. Only one cell K is involved in the computation of each local tensor when the finite element spaces U^1 and U^2 are defined over the same reference element. The indices c^i are the indices of this integration cell K in the corresponding submeshes $\mathcal{T}^i$ (see Figure 4). The computation of these indices from the mesh mappings is shown in Listing 12.

```
// Codimension 0 : C^i → C^j
cell_index[i][0] = mapping->cell_map()[cell->index()];
```

Listing 12. [C++] Each index c^i (`cell_index[i][0]`) of the integration mesh cell K (`cell`) relative to the basis function space mesh $\mathcal{T}^i$ is computed from the cell maps provided by the corresponding `MeshView` object `mapping`.

As described in Section 6 the cell assembly algorithm iterates over the cells K of the integration domain $\mathcal{K}$ (`mesh`). The computation of the local tensor A^K relative to the integration mesh cell K use the standard implementation of `tabulate_tensor` kernel as given in Section 7.1. The indices m and n (e.g. in the case of bilinear forms) of the global degrees of freedom in the function spaces U^i for $i = 1, 2$ (`i = 0, 1`) are obtained from the local-to-global mappings ι^i (`dofmaps[i].cell_dofs`) (28).

```
for (CellIterator cell(mesh); !cell.end(); ++cell)
{
  // Compute local element tensor A^K (ufc.A)
  integral->tabulate_tensor(ufc.A.data(), ...);
  // Compute m = ι^1_{c^1}(l_1) and n = ι^2_{c^2}(l_2)
  for(std::size_t i=0; i<form_rank; ++i)
  {
    auto dmap = dofmaps[i]->cell_dofs(cell_index[i][0]);
    dofs[i].set(dmap.size(), dmap.data());
  }
  // Add A^K to A
  A.add_local(ufc.A.data(), dofs);
}
```

Listing 13. [C++] The homogeneous dimension cell assembly involves standard local tensor computation using `tabulate_tensor`. The local-to-global mappings $\iota^i_{c^i}$ are defined from the local-to-global mappings `dofmaps[i].cell_dofs` to which we give the appropriate cell index `cell_index[i][0]` relative to $\mathcal{T}^i$.

7.2.2 Case 2 (codimension one) $d^{\mathcal{K}} = d^2 = d^1 - 1$. The codimension one cell assembly involves the star S_K of the integration mesh cell K (see Figure 4). The computation of the indices (`cell_index[i][j]`) of the cells K^j in the star S_K via the submesh mappings and the mesh connectivity is shown in Listing 14. The local index of K viewed as a facet relative to K^j (`local_facets[j]`), required by the revised `tabulate_tensor` implementation, can also be derived from the mesh connectivity.

```
// Codimension 1 : C^i → F^j → {C^j, C^j}
Facet f(*(mapping->mesh()),mapping->cell_map()[cell->index()]);
// Building S_K as cells K̃ (dim D) that are adjacent to f
const std::size_t D = mapping->mesh()->topology().dim();
for(std::size_t j=0; j<f.num_entities(D);j++)
{
  Cell mesh_cell(*(mapping->mesh()), f.entities(D)[j]);
  cell_index[i][j] = mesh_cell.index());
  // Local index of facet f in mesh_cell
  local_facets.push_back(mesh_cell.index(f));
}
```

Listing 14. [C++] The index c^i (`cell_index[i][j]`) of $K^j \in S_K$ relative to $\mathcal{T}^i$ is obtained from the set of cells adjacent to the corresponding facet `f` in the higher dimensional mesh. The local index of this facet in the cell K^j (`local_facets[j]`) is required to compute the local tensors $A^{K^j,K}$.

As detailed in Algorithm 2, the assembly over mixed dimensions involves an additional loop over the cells $\tilde{K}$ in S_K. The local tensors $A^{\tilde{K},K}$ are computed from the revised `tabulate_tensor` function taking the local index of the corresponding facet as an additional argument (see Section 7.1). Again, the indices m and n (e.g. in the case of bilinear forms) of the global degrees of freedom in the function spaces U^i for $i = 1, 2$ (`i = 0, 1`) are obtained from the local-to-global mappings ι^i (`dofmaps[i].cell_dofs`) (28). As specified in Section 6, entries of the local tensors $A^{\tilde{K},K}$ may have to be zeroed to avoid duplicates.

```
for (CellIterator cell(mesh); !cell.end(); ++cell)
{
  // Iterating over cells K̃ in S_K
  for(std::size_t j=0; j<local_facets.size(); ++j)
  {
    // Compute A^{K̃,K}
    integral->tabulate_tensor(ufc.A.data(),...,local_facets[j]);
    // Compute m = ι^1_{c^1}(l_1) and n = ι^2_{c^2}(l_2)
    for(std::size_t i=0; i<form_rank; ++i)
    {
      std::size_t jidx = (cell_index[i].size() > 1) ? j:0;
      auto dmap = dofmaps[i]->cell_dofs(cell_index[i][jidx]);
      zero(dmap, ...);
      dofs[i].set(dmap.size(), dmap.data());
    }
    // Add entry (l_1, l_2) of A^{K̃,K} to A
    A.add_local(ufc.A.data(), dofs);
  }
}
```

Listing 15. [C++] The codimension one assembly iterates over the cells K of the integration domain and the cells $\tilde{K}$ of its star S_K. The local tensors $A^{\tilde{K},K}$ are computed from the revised `tabulate_tensor` taking the local index of the facet (`local_facets[j]`) as an additional argument. The local-to-global mappings $\iota^i_{c^i}$ are defined from the degrees of freedom mappings `dofmaps[i].cell_dofs` with the index `cell_index[i][j]` of the j^{th} cell $\tilde{K} \in S_K$ relative to $\mathcal{T}^i$.

7.3 Block linear algebra and representing assembled tensors

Once assembled as described in Section 6, the block tensors are recombined to form the block systems (12) and (20). The FEniCS/DOLFIN library [33, 34] uses the software package PETSc [4] for linear algebra objects and algorithms.

In particular, the PETSc `MATNEST` structure is dedicated to efficient representation and use of block tensors. This PETSc data structure has been interfaced in FEniCS/DOLFIN as a `PETScNestMatrix` class building a `MATNEST` object from a list of matrices, cf. Listing 16. The `PETScNestMatrix` class is also equipped with a `init_vectors` function for building vectors with the appropriate block structure.

```
A = PETScNestMatrix([A_00, ..., A_NN]);
b = Vector()
A.init_vectors(b, [b_0, ..., b_N]);
```

Listing 16. [Python] The assembled blocks are combined into a single block tensor of type `PETScNestMatrix` which interfaces the dedicated PETSc data structure `MATNEST`. The right hand side block vector `b` is built from `A` using the `init_vectors` function with a matching structure.

The wide selection of solvers and preconditioners available in FEniCS/DOLFIN via PETSc can be applied to `PETScNestMatrix` objects in the same manner as with standard single domain system. However, direct solvers are not directly compatible with this data structure. Instead, `PETScNestMatrix` objects can easily be converted from the `MATNEST` format to the more standard `MATAIJ` format using the function `convert_to_aij` interfacing the corresponding PETSc routine (see Listing 17).

```
# Solve block system using iterative solver
solver = PETScKrylovSolver()
solver.solve(A, x, b);

# Solve block system using direct solver
solver = PETScLUSolver()
A.convert_to_aij()
solver.solve(A, x, b);
```

Listing 17. [Python] The recombined block system $Ax = b$ can be solved using e.g. iterative or direct solvers.

Moreover, the `MATNEST` data structure is compatible with the `PCFieldSplit` preconditioners offered by PETSc, allowing for the application of specific preconditioners to each block matrix.

8 NUMERICAL RESULTS

The presented framework is applicable to a wide range of mixed dimensional problems. In this section, we report on numerical results for three selected cases. We start with the reference Poisson problem introduced in Section 1 as a demonstration of the described features. Second, we study two Stokes problems with non-standard boundary conditions as discussed in [7, 46]. Finally, we

consider a mathematical model of ionic electrodiffusion in brain tissue. Our software to reproduce the presented results is openly and freely available (see [16, 17])

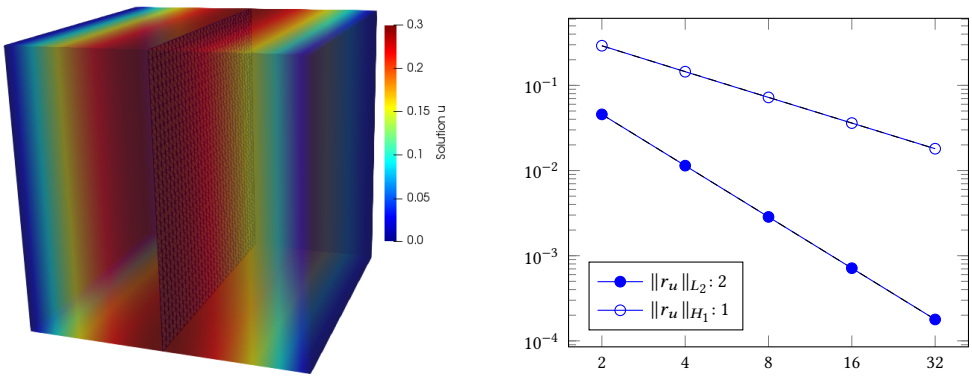
8.1 Reference Poisson problem

This numerical experiment presents a convergence study performed on the 3D version of Example 1 using the method of manufactured solutions. The function $u(x, y) = x(1 - x)$ is the exact solution of Example 1 with $f = 2$ and $c = 0.25$. We consider a uniform tetrahedral mesh $\mathcal{T}^1$ of the unit cube, and find the approximations u_h using the space of continuous piecewise linear polynomials U^1 relative to this mesh and c_h using continuous piecewise linear polynomials defined relative to a mesh $\mathcal{T}^2$ of the two-dimensional midplane. The obtained solution is shown in Figure 8a.

We introduce the approximation error e_h defined as $e_h = u - u_h$. Given k the polynomial order associated with $U^1(\mathcal{T}^1)$, and h the mesh size, there exists a constant $\alpha > 0$ such that

$$\|e_h\|_{L_2} \leqslant \alpha h^{k+1} \text{ and } \|e_h\|_{H_1} \leqslant \alpha h^k. \tag{38}$$

Figure 8b plots the L_2 and H_1 norms of the approximation error with respect to the mesh resolution, for the case $k = 1$. The slope of the corresponding lines – indicated in legend – shows that the expected orders of convergence (38) are obtained.



(a) Solution u_h (b) Convergence study

Fig. 8. Solution of the Poisson problem given in Example 1 with $f = 2$ and $c = 0.25$ to obtain the manufactured solution $u(x, y) = x(1 - x)$, and the corresponding convergence study plotting $\|e_h\|_{L_2}$ and $\|e_h\|_{H_1}$ with order $k = 1$ depending on the mesh resolution. $\|r_u\|_{L_2}$ and $\|r_u\|_{H_1}$ are the resulting convergence rates.

8.2 Fluid flow problems with non-standard boundary conditions

8.2.1 A Stokes-Brinkman problem with a manufactured solution. We consider the Stokes-Brinkman problem (39) solved on the domain $\Omega = [0, 1] \times [0, 1]$.

$$\begin{aligned} -\Delta u + u - \nabla p &= f \text{ on } \Omega, \\ \nabla \cdot u &= 0 \text{ on } \Omega. \end{aligned} \tag{39}$$

We introduce the manufactured solutions u and p (40) from which the right hand side f in (39) and the boundary conditions (41) are defined as

$$u = \begin{pmatrix} \cos(\pi y) \sin(\pi x) \\ -\cos(\pi x) \sin(\pi y) \end{pmatrix}, \quad p = \pi \cos(\pi x) \cos(\pi y). \tag{40}$$

We denote by Γ_t and Γ_b the top and bottom boundaries, respectively, on which we impose homogeneous Neumann conditions. Further, we set the velocity g at the inlet boundary Γ_{in} to

be the manufactured solution $u|_{\Gamma_{\text{in}}}$, imposed through a Lagrange multiplier $\lambda \in \Gamma_{\text{in}}$. In addition, a inhomogeneous Neumann condition is imposed on Γ_{out}, with traction h defined from (40):

$$\nabla u \cdot n + pn = h \text{ on } \Gamma_{\text{out}}. \tag{41}$$

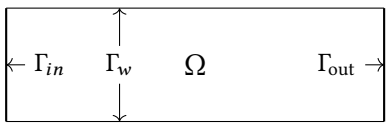
Combining, we obtain a mixed dimensional problem with the variational formulation: find $(u, p, \lambda) \in U \times P \times L$ such that

$$\begin{aligned} \int_\Omega \nabla u \cdot \nabla v + u \cdot v + p \nabla \cdot v + q \nabla \cdot u \, \mathrm{d}x + \int_{\Gamma_{\text{in}}} \lambda \cdot v + \eta \cdot u \, \mathrm{d}s \\ = \int_\Omega f \cdot v \, \mathrm{d}x + \int_{\Gamma_{\text{out}}} h \cdot v \, \mathrm{d}s + \int_{\Gamma_{\text{in}}} \eta \cdot g \, \mathrm{d}s, \end{aligned} \tag{42}$$

for all $(v, q, \eta) \in U \times P \times L$. We define a uniform mesh of the unit square $\mathcal{T}^1$, and a lower-dimensional mesh $\mathcal{T}^2$ of the boundary Γ_{in}. The velocity u is approximated as $u_h \in U$ through continuous piecewise vector fields of polynomial order $k + 1 \geq 2$ while continuous piecewise polynomials of order $k \geq 1$ are used for the pressure approximation $p_h \in P$. The Lagrange multiplier λ is approximated in the space $L = L(\mathcal{T}^2)$ of continuous piecewise polynomials of order k defined relative to $\mathcal{T}^2$.

Iterative solvers, such as e.g. gmres with ilu preconditioning, easily fail to converge for this problem due to the ill-conditioning of the system. A fractional preconditioning strategy was introduced in [28]. In Figure 9, we demonstrate that we obtain the expected order of convergence (38), both using a direct solver and using said preconditioning technique, for $k = 1, 2$.

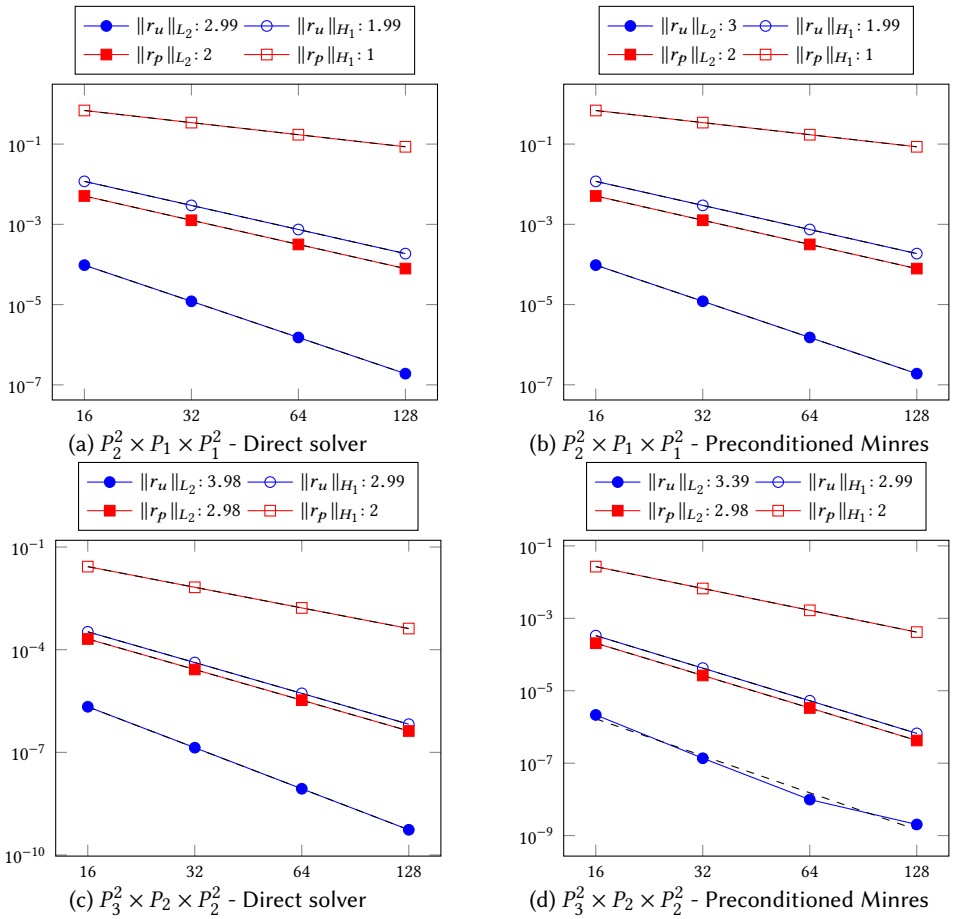
8.2.2 A Stokes problem with non-standard traction conditions. The next test case presents the a variant of the Stokes problem (see Figure 10) discussed in [7, 46], involving non-standard traction boundary conditions at the inlet and outlet boundaries Γ_{in} and Γ_{out}, respectively. This precise formulation involving the symmetric velocity gradient may be useful in connection with e.g. fluid-structure interaction problems[7].



$$-\mu\nabla(\nabla u + \nabla u^T) + \nabla p = f \text{ on } \Omega$$
$$\nabla \cdot u = 0 \text{ on } \Omega$$
$$u \times n = 0 \text{ on } \Gamma_{\text{in}} \cup \Gamma_{\text{out}}$$

Fig. 10. The domain Ω (left) is the rectangle $[0, 10] \times [0.5]$ where Γ_{in} and Γ_{out} represent the inlet and the outlet, and Γ_w denotes the upper and lower boundaries (representing horizontal walls). The equations (right) are based on a standard formulation of the Stokes equations with additional traction conditions on Γ_{in} and Γ_{out}.

The traction conditions are imposed using a Lagrange multiplier λ_{in} (resp. λ_{out}) relative to the inlet Γ_{in} (resp. the outlet Γ_{out}), acting on the tangential component of the velocity $u \cdot t \equiv u \times n$. The standard no-slip condition $u = 0$ is applied to the walls Γ_w, and a pressure difference is imposed between the inlet where $p = p_{\text{in}}$ and the outlet where we impose $p = p_{\text{out}}$. We also apply homogeneous Dirichlet boundary conditions for both Lagrange multipliers λ_i and λ_{out}.



(a) $P_2^2 \times P_1 \times P_1^2$ - Direct solver

(b) $P_2^2 \times P_1 \times P_1^2$ - Preconditioned Minres

(c) $P_3^2 \times P_2 \times P_2^2$ - Direct solver

(d) $P_3^2 \times P_2 \times P_2^2$ - Preconditioned Minres

Fig. 9. Convergence study for the Stokes-Brinkman problem (39). The plots show the approximation error $\|e_h\|_Q$ (38) in the Q norm depending on the mesh resolution. $\|r_v\|_Q$ defines the rate of convergence for the solution variable v in the Q norm. (a) and (b) show that the $P_2^2 \times P_1 \times P_1^2$ approximation gives the expected convergence rates in the L_2 and H_1 norms, both using a direct solver and a preconditioned [28] iterative solver. (c) and (d) show that the expected convergence rates are still obtained with higher order elements $P_3^2 \times P_2 \times P_2^2$.

The variational formulation then reads: find $(u, p, \lambda_{\text{in}}, \lambda_{\text{out}}) \in U \times P \times L_{\text{in}} \times L_{\text{out}}$ such that

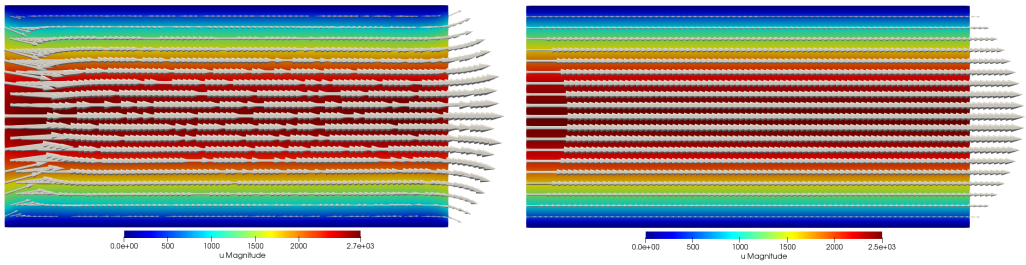
$$\begin{aligned} \mu \int_\Omega (\nabla u \quad &+ \quad \nabla u^T) \cdot (\nabla v + \nabla v^T) - p(\nabla \cdot v) - q(\nabla \cdot u)\, \mathrm{d}x \\ &+ \quad \int_{\Gamma_{\text{in}}} \lambda_{\text{in}}(v \times n) + \eta_{\text{in}}(u \times n)\, \mathrm{d}s + \int_{\Gamma_{\text{out}}} \lambda_{\text{out}}(v \times n) + \eta_{\text{out}}(u \times n)\, \mathrm{d}s \\ &= \quad \int_\Omega f \cdot v - \int_{\Gamma_{\text{in}}} p_{\text{in}}(v \cdot n) - \int_{\Gamma_{\text{out}}} p_{\text{out}}(v \cdot n) \end{aligned} \tag{43}$$

for all $(v, q, \eta_{\text{in}}, \eta_{\text{out}}) \in U \times P \times L_{\text{in}} \times L_{\text{out}}$.

Again, we define a uniform mesh $\mathcal{T}^1$ of the domain Ω and lower-dimensional meshes $\mathcal{T}^2, \mathcal{T}^3$ for the boundaries Γ_{in}, Γ_{out}, respectively. The approximation of the velocity u and the pressure p of (43) uses the standard Taylor-Hood elements, *i.e.* second order (resp. first order) Lagrange finite

elements for $u \in U$ (resp. for $p \in P$). The Lagrange multipliers are defined in continuous piecewise quadratic function spaces $L_{\text{in}} = L_{\text{in}}(\mathcal{T}^2)$ and $L_{\text{out}} = L_{\text{out}}(\mathcal{T}^3)$, ensuring the well posedness of the problem as detailed in [46].

Figure 11 compares the results obtained with and without the traction condition, i.e. with and without the use of the Lagrange multipliers. Both solutions were computed through the presented framework and preconditioned with the fractional preconditioner [28] introduced in Section 8.2.1.



(a) Without traction condition (b) With traction condition

Fig. 11. Comparison between the velocity field obtained from the Stokes problem with standard boundary conditions i.e. without the Lagrange multipliers and the velocity field obtained with the traction condition on the inlet and the outlet. All other variables (mesh, material parameters etc.) were kept fixed.

8.3 Ionic electrodiffusion in cellular geometries

Many cerebral pathological conditions e.g. spreading depression and epilepsy [45] are associated with changes in ion concentrations in the brain tissue. In this last example, we consider a model of ionic electrodiffusion in intracellular and extracellular domains, separated by a cell membrane. We represent the intracellular and extracellular domains as separate two-dimensional subdomains with the cell membrane as a topologically one-dimensional submesh. For more details of the mathematical model and numerical method, we refer to [18].

For this specific test case, illustrated in Figure 12, we consider a domain $\Omega \subset \mathbb{R}^2$ consisting of $\Omega_i \subset \mathbb{R}^2$ and $\Omega_e \subset \mathbb{R}^2$ representing the intracellular and extracellular spaces, respectively, together with the cell membrane $\Gamma = \bar{\Omega}_i \cap \bar{\Omega}_e$. The unknowns are the ion concentrations $[k]_i$ (resp. $[k]_e$) for each ion species $k \in K = \{\text{Na}^+, \text{K}^+, \text{Cl}^-\}$, the electrical potential ϕ_i (resp. ϕ_e) in the intracellular space Ω_i (resp. extracellular space Ω_e), and the total ionic current density I_M at the (lower dimensional) cell membrane Γ.

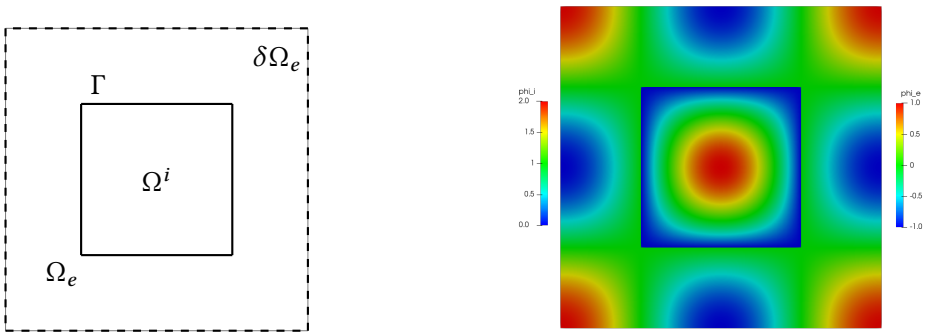


Fig. 12. Illustration of the domain composed of the extra cellular space Ω_e, the intra cellular space Ω_i and the membrane Γ as their interface (left). First order approximation of the potentials $\phi_i \in \Omega_i$ and $\phi_e \in \Omega_e$ matching the manufactured solution (50) (right).

The evolution and distribution of the ion concentration $[k]_r$, $r = \{i, e\}$ for $k \in K$ is described by the continuity equation

$$\frac{\partial [k]_r}{\partial t} + \nabla \cdot J_r^k = f_r \text{ in } \Omega_r. \tag{44}$$

The ion flux density J_r^k ($r = \{i, e\}$) is expressed in terms of the ion concentration gradients $\nabla [k]_r$ for $k \in K$ and the electrical potential gradients $\nabla \phi_r$ as

$$J_r^k = -D_r^k \nabla [k]_r - \frac{D_r^k z^k}{\psi} [k]_r \nabla \phi_r \tag{45}$$

where D_r^k, $r = \{i, e\}$ is the effective diffusion coefficient and z^k the valence of the ion species $k \in K$. $\psi = RTF^{-1}$ with F the Faraday's constant, T is the absolute temperature, and R the gas constant. Moreover, these ion flux densities are assumed to satisfy the electroneutrality assumption:

$$F \sum_{k \in K} z^k \nabla \cdot J_r^k = 0 \text{ in } \Omega_r \ \forall r \in \{i, e\} \tag{46}$$

Assuming that no charge can leave or enter the system yields the exterior boundary condition

$$F \sum_{k \in K} z^k J_e^k \cdot n_e = 0 \text{ on } \delta\Omega_e. \tag{47}$$

The transmembrane potential is introduced as the difference between the intracellular and extracellular potential $\phi_M = \phi_i - \phi_e$ at the cell membrane, which satisfies

$$\frac{\partial \phi_M}{\partial t} = \frac{1}{C_M}(I_M - I_{ch}) \tag{48}$$

where C_M and I_{ch} are the given capacitance and ion species specific channel current, respectively. This additional equation (48) giving the total ionic current density $I_M \in \Gamma$ is coupled with (44) by the conservation equation of I_M over the cell membrane as

$$-F \sum_{k \in K} z^k J_i^k \cdot n_i = F \sum_{k \in K} z^k J_e^k \cdot n_e \equiv I_M. \tag{49}$$

We introduce manufactured solutions $[k]_r$, $k \in K$ for the ion concentrations and ϕ_r for the electric potential ($r = \{i, e\}$) satisfying (44)-(49) on $\Omega = \Omega_i \cup \Omega_e = [0, 1] \times [0, 1]$.

$$\begin{aligned}
\text{Na}_i &= 0.7 + 0.3 \sin(2\pi x) \sin(2\pi y)(1 + e^{-t}) \\
\text{Na}_e &= 1.0 + 0.6 \sin(2\pi x) \sin(2\pi y)(1 + e^{-t}) \\
\text{K}_i &= 0.3 + 0.3 \sin(2\pi x) \sin(2\pi y)(1 + e^{-t}) \\
\text{K}_e &= 1.0 + 0.2 \sin(2\pi x) \sin(2\pi y)(1 + e^{-t}) \\
\text{Cl}_i &= 1.0 + 0.6 \sin(2\pi x) \sin(2\pi y)(1 + e^{-t}) \\
\text{Cl}_e &= 2.0 + 0.8 \sin(2\pi x) \sin(2\pi y)(1 + e^{-t}) \\
\phi_i &= \cos(2\pi x) \cos(2\pi y)(1 + e^{-t}) \\
\phi_e &= \cos(2\pi x) \cos(2\pi y)
\end{aligned} \tag{50}$$

As our test case here, we then consider the boundary conditions and sources induced by inserting the manufactured solution (50) into (44)-(49).

We define a uniform mesh $\mathcal{T}^1$ of the unit square Ω, from which we build two two-dimensional meshes $\mathcal{T}^2$ and $\mathcal{T}^3$ relative to the intracellular domain Ω_i and the extracellular domain Ω_e, respectively. We consider a lower-dimensional mesh $\mathcal{T}^4$ to define the cell membrane Γ. All the unknowns in our system i.e. the ion concentrations $[k]_r, r = \{i, e\}, k = \{\text{Na}^+, \text{K}^+, \text{Cl}^-\}$ and the

electrical potentials ϕ_i and ϕ_e, are approximated using piecewise continuous elements of order $l \geq 1$.

The corresponding solutions for the electrical potentials ϕ_i and ϕ_e are shown in Figure 12. A convergence study of the error of the approximation in the L_2 and H_1 norms for the Sodium (Na^+) concentrations and electrical potentials ϕ_i, ϕ_e is shown in Figure 13. The convergence rates indicate that we obtain an expected order of convergence (38) for both polynomial orders $l = \{1, 2\}$. The analogous results are obtained for the other ion concentrations.

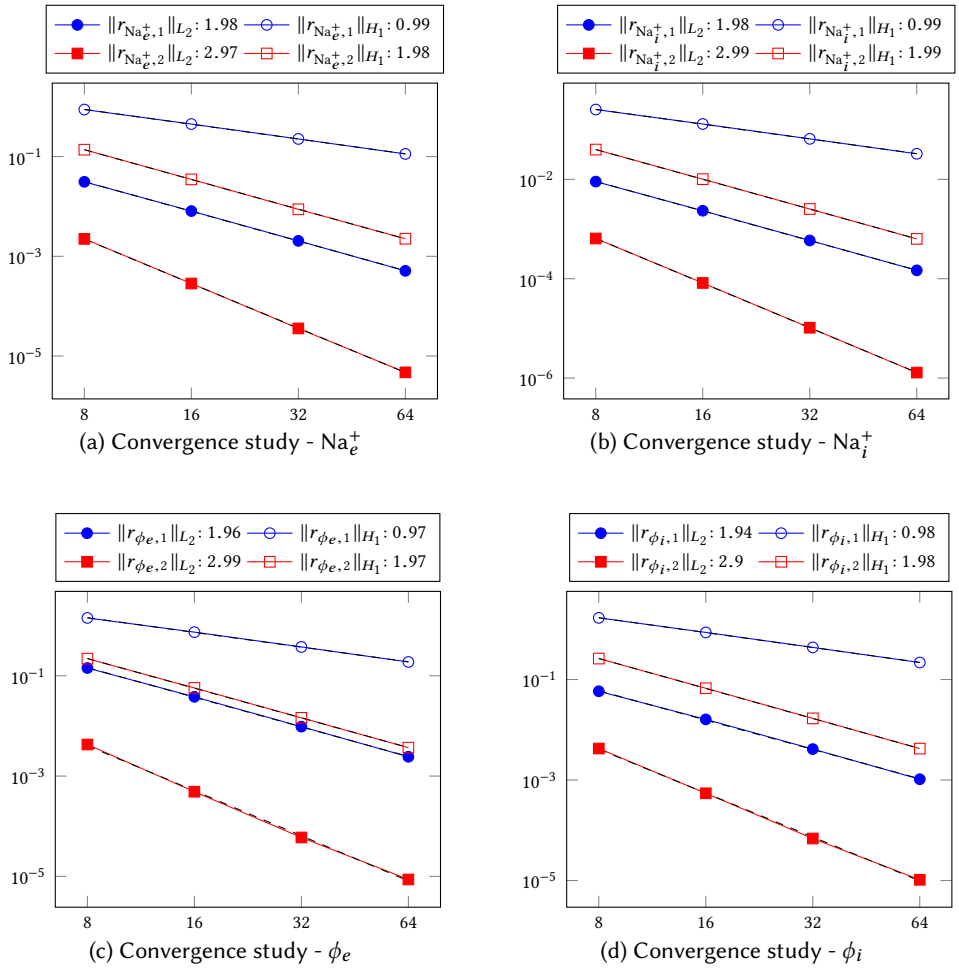


Fig. 13. Convergence study for the KNP-EMI model given by (44)-(49) based on the manufactured solution (50). The plots show the approximation error $\|e_h\|_Q$ (38) in the Q norm depending on the mesh resolution. $\|r_{v,l}\|_Q$ defines the rate of convergence for the solution variable v in the Q norm with approximation order l. The resulting convergence rates are given in legend. The expected convergence rates in L_2 and H_1 norms are obtained for both first and second order approximations of sodium (Na^+) concentration (a)-(b) and for the electric potentials ϕ_e (c) and ϕ_i (d).

9 CONCLUSIONS

We have introduced a set of abstractions, algorithms and design guidelines for the automated assembly and solution of mixed domain and mixed dimensional finite element methods. Further, we

have presented a realization of these general concepts within the FEniCS finite element software. These features thus allow for the solution of PDEs posed on different domains, either of the same dimension or involving codimension one subdomains. We have illustrated the features with a number of numerical examples starting from a basic constrained Poisson problem to a nontrivial model of ionic electrodiffusion. However, we argue that this series of examples only begin to illustrate the possibilities offered by the framework. Future work will focus on the extension of the framework to coupled problems with higher codimensions, non-conforming meshes, and optimal mesh partitioning.

ACKNOWLEDGMENTS

This project has received funding from the European Research Council (ERC) under the European Union's Horizon 2020 research and innovation programme under grant agreement 714892 (Waterscales).

We thank Martin Alnæs, Miroslav Kuchta and Jørgen Dokken (Simula Research Laboratory) for constructive discussion on topics related to the manuscript.

REFERENCES

[1] Martin S. Alnæs, Jan Blechta, Johan Hake, August Johansson, Benjamin Kehlet, Anders Logg, Chris Richardson, Johannes Ring, Marie E. Rognes, and Garth N. Wells. 2015. The FEniCS Project Version 1.5. *Archive of Numerical Software* 3, 100 (2015), 9–23. https://doi.org/10.11588/ans.2015.100.20553

[2] Martin S. Alnæs, Anders Logg, Kristian B. Ølgaard, Marie E. Rognes, and Garth N. Wells. 2014. Unified Form Language: A Domain-specific Language for Weak Formulations of Partial Differential Equations. *ACM Trans. Math. Softw.* 40, 2, Article 9 (March 2014), 37 pages. https://doi.org/10.1145/2566630

[3] Douglas N. Arnold, Franco Brezzi, Bernardo Cockburn, and Donatella Marini. 2000. Discontinuous Galerkin Methods for Elliptic Problems. In *Discontinuous Galerkin Methods*, Bernardo Cockburn, George E. Karniadakis, and Chi-Wang Shu (Eds.). Springer Berlin Heidelberg, Berlin, Heidelberg, 89–101.

[4] Satish Balay, Shrirang Abhyankar, Mark F. Adams, Jed Brown, Peter Brune, Kris Buschelman, Lisandro Dalcin, Victor Eijkhout, William D. Gropp, Dinesh Kaushik, Matthew G. Knepley, Dave A. May, Lois Curfman McInnes, Richard Tran Mills, Todd Munson, Karl Rupp, Patrick Sanan, Barry F. Smith, Stefano Zampini, Hong Zhang, and Hong Zhang. 2018. PETSc Web page. http://www.mcs.anl.gov/petsc. http://www.mcs.anl.gov/petsc

[5] F Ballarin. Accessed: 2018-10-16. multiphenics - easy prototyping of multiphysics problems in FEniCS. https://mathlab.sissa.it/multiphenics.

[6] W. Bangerth, R. Hartmann, and G. Kanschat. 2007. deal.II – a General Purpose Object Oriented Finite Element Library. *ACM Trans. Math. Softw.* 33, 4 (2007), 24/1–24/27.

[7] S. Bertoluzza, V. Chabannes, C. PrudâĂŹhomme, and M. Szopos. 2017. Boundary conditions involving pressure for the Stokes problem and applications in computational hemodynamics. *Computer Methods in Applied Mechanics and Engineering* 322 (2017), 58 – 80. https://doi.org/10.1016/j.cma.2017.04.024

[8] Wietse Marijn Boon. 2018. *Conforming Discretizations of Mixed-Dimensional Partial Differential Equations.* Doctoral thesis. University of Bergen. http://bora.uib.no/handle/1956/18159

[9] Wietse M. Boon, Jan M. Nordbotten, and Jon E. Vatne. 2017. Functional Analysis and Exterior Calculus on Mixed-Dimensional Geometries. arXiv:math.AP/1710.00556

[10] S. Brenner and R. Scott. 2007. *The Mathematical Theory of Finite Element Methods.* Springer New York, 233 Spring St, New York, NY 10013, USA. https://books.google.no/books?id=ci4c_R0WKYYC

[11] Franco Brezzi, Jim Douglas, and L Donatella Marini. 1985. Two families of mixed finite elements for second order elliptic problems. *Numer. Math.* 47, 2 (1985), 217–235.

[12] Erik Burman, Susanne Claus, Peter Hansbo, Mats G. Larson, and AndrÃĪ Massing. 2015. CutFEM: Discretizing geometry and partial differential equations. *Internat. J. Numer. Methods Engrg.* 104, 7 (2015), 472–501. https://doi.org/10.1002/nme.4823 arXiv:https://onlinelibrary.wiley.com/doi/pdf/10.1002/nme.4823

[13] Sunčica Čanić, Marija Galić, Matko Ljulj, Boris Muha, Josip Tambača, and Yifan Wang. 2019. Analysis of a linear 3D fluid–mesh–shell interaction problem. *Zeitschrift für angewandte Mathematik und Physik* 70, 2 (18 Feb 2019), 44. https://doi.org/10.1007/s00033-019-1087-1

[14] P. G. Ciarlet. 1976. Numerical Analysis of the Finite Element Method.

[15] P. G. Ciarlet. 2002. *The Finite Element Method for Elliptic Problems.* Society for Industrial and Applied Mathematics, USA. https://books.google.no/books?id=isEEyUXW9qkC

[16] Cécile Daversin-Catty, Chris N. Richardson, Ada J. Ellingsrud, and Marie E. Rognes. 2019. Docker container for mixed dimensional FEniCS branches. https://hub.docker.com/r/ceciledc/fenics_mixed_dimensional (tag: v2019.1).

[17] Cécile Daversin-Catty, Chris N. Richardson, Ada J. Ellingsrud, and Marie E. Rognes. 2019. Mixed-dimensional-examples v2019.1. https://zenodo.org/record/3525001. https://doi.org/10.5281/zenodo.3525001

[18] A. J. Ellingsrud, A. Solbrå, G. T. Einevoll, G. Halnes, and M. E. Rognes. 2019. Finite element simulation of ionic electrodiffusion in cellular geometries. (2019).

[19] A. Ern and J.L. Guermond. 2004. *Theory and Practice of Finite Elements.* Springer New York, 233 Spring St, New York, NY 10013, USA. https://books.google.no/books?id=CCjm79FbJbcC

[20] Patrick E Farrell, David A Ham, Simon W Funke, and Marie E Rognes. 2013. Automated derivation of the adjoint of high-level transient finite element programs. *SIAM Journal on Scientific Computing* 35, 4 (2013), C369–C393.

[21] F. Hecht. 2012. New development in FreeFem++. *J. Numer. Math.* 20, 3-4 (2012), 251–265.

[22] Luca Heltai and Francesco Costanzo. 2012. Variational implementation of immersed finite element methods. *Computer Methods in Applied Mechanics and Engineering* 229-232 (2012), 110 – 127. https://doi.org/10.1016/j.cma.2012.04.001

[23] KE Holter, M Kuchta, and KA Mardal. 2017. Trace Constrained Problems in FEniCS. https://doi.org/10.6084/m9.figshare.5086369

[24] August Johansson, Benjamin Kehlet, Mats G. Larson, and Anders Logg. 2019. Multimesh finite element methods: Solving PDEs on multiple intersecting meshes. *Computer Methods in Applied Mechanics and Engineering* 343 (2019), 672 – 689. https://doi.org/10.1016/j.cma.2018.09.009

[25] George Karypis. 2011. METIS and ParMETIS. In *Encyclopedia of Parallel Computing*. Springer, New York, 1117–1124. https://doi.org/10.1007/978-0-387-09766-4_500

[26] Eirik Keilegavlen, Alessio Fumagalli, Runar Berge, Ivar Stefansson, and Inga Berre. 2017. PorePy: An Open-Source Simulation Tool for Flow and Transport in Deformable Fractured Rocks. arXiv:cs.CE/1712.00460

[27] Timo Koch, Katharina Heck, Natalie Schröder, Holger Class, and Rainer Helmig. 2018. A New Simulation Framework for Soil-Root Interaction, Evaporation, Root Growth, and Solute Transport. *Vadose zone journal* 17, 1 (2018), 0 –. https://doi.org/10.2136/vzj2017.12.0210

[28] Miroslav Kuchta, Magne Nordaas, Joris C. G. Verschaeve, Mikael Mortensen, and Kent-Andre Mardal. 2016. Preconditioners for Saddle Point Systems with Trace Constraints Coupling 2D and 1D Domains. *SIAM Journal on Scientific Computing* 38, 6 (2016), B962–B987. https://doi.org/10.1137/15M1052822

[29] Martin Werner Licht. 2017. Complexes of Discrete Distributional Differential Forms and Their Homology Theory. *Found. Comput. Math.* 17, 4 (Aug. 2017), 1085–1122. https://doi.org/10.1007/s10208-016-9315-y

[30] A. Logg. 2009. Efficient Representation of Computational Meshes. *Int. J. Comput. Sci. Eng.* 4, 4 (Nov. 2009), 283–295. https://doi.org/10.1504/IJCSE.2009.029164

[31] Anders Logg, Kent-Andre Mardal, Garth N. Wells, et al. 2012. *Automated Solution of Differential Equations by the Finite Element Method.* Springer, Berlin, Heidelberg. https://doi.org/10.1007/978-3-642-23099-8

[32] Anders Logg, Kristian B. Ølgaard, Marie E. Rognes, and Garth N. Wells. 2012. *FFC: the FEniCS Form Compiler.* Springer, Berlin, Heidelberg, Chapter 11, 227–238.

[33] Anders Logg and Garth N. Wells. 2010. DOLFIN: Automated Finite Element Computing. *ACM Trans. Math. Softw.* 37, 2, Article 20 (April 2010), 28 pages. https://doi.org/10.1145/1731022.1731030

[34] Anders Logg, Garth N. Wells, and Johan Hake. 2012. *DOLFIN: a C++/Python Finite Element Library.* Springer, Berlin, Heidelberg, Chapter 10, 173–225.

[35] J. -C Nédélec. 1980. Mixed finite elements in $\mathbb{R}^3$. *Numer. Math.* 35, 3 (1980), 315–341.

[36] J. -C Nédélec. 1986. A new family of mixed finite elements in $\mathbb{R}^3$. *Numer. Math.* 50, 1 (1986), 57–81.

[37] François Pellegrini and Jean Roman. 1996. Scotch: A software package for static mapping by dual recursive bipartitioning of process and architecture graphs. In *High-Performance Computing and Networking*. Springer Berlin Heidelberg, Berlin, Heidelberg, 493–498.

[38] Christophe Prud'Homme, Vincent Chabannes, Vincent Doyeux, Mourad Ismail, Abdoulaye Samake, and Gonçalo Pena. 2012. Feel++: A Computational Framework for Galerkin Methods and Advanced Numerical Methods. *ESAIM: Proceedings* 38 (Dec. 2012), 429–455. https://doi.org/10.1051/proc/201238024

[39] Florian Rathgeber, David A. Ham, Lawrence Mitchell, Michael Lange, Fabio Luporini, Andrew T. T. Mcrae, Gheorghe-Teodor Bercea, Graham R. Markall, and Paul H. J. Kelly. 2016. Firedrake: Automating the Finite Element Method by Composing Abstractions. *ACM Trans. Math. Softw.* 43, 3, Article 24 (Dec. 2016), 27 pages. https://doi.org/10.1145/2998441

[40] P. -A. Raviart and J. M. Thomas. 1977. A mixed finite element method for 2nd order elliptic problems. In *Mathematical aspects of finite element methods (Proc. Conf., Consiglio Naz. delle Ricerche (C.N.R.), Rome, 1975).* Springer, Berlin, 292–315. Lecture Notes in Math., Vol. 606.

[41] M. E. Rognes, D. A. Ham, C. J. Cotter, and A. T. T. McRae. 2013. Automating the solution of PDEs on the sphere and other manifolds in FEniCS 1.2. *Geoscientific Model Development* 6, 6 (2013), 2099–2119. https://doi.org/10.5194/gmd-6-2099-2013

[42] Abdoulaye Samake. 2014. *Large scale nonconforming domain decomposition methods.* Theses. Université Grenoble Alpes. https://tel.archives-ouvertes.fr/tel-01092968

[43] J. Schöberl. 2019. NGSolve Finite Element Library. https://sourceforge.net/projects/ngsolve/

[44] Nicolas Schwenck, Bernd Flemisch, Rainer Helmig, and Barbara I. Wohlmuth. 2015. Dimensionally reduced flow models in fractured porous media: crossings and boundaries. *Computational Geosciences* 19, 6 (01 Dec 2015), 1219–1230. https://doi.org/10.1007/s10596-015-9536-1

[45] George G. Somjen. 2001. Mechanisms of Spreading Depression and Hypoxic Spreading Depression-Like Depolarization. *Physiological Reviews* 81, 3 (2001), 1065–1096. https://doi.org/10.1152/physrev.2001.81.3.1065 PMID: 11427692.

[46] Marcela Szopos. 2017. *Mathematical modeling, analysis and simulations for fluid mechanics and their relevance to in silico medicine.* Habilitation à diriger des recherches. Université de Strasbourg, IRMA UMR 7501. https://tel.archives-ouvertes.fr/tel-01646867

[47] Aslak Tveito, Karoline H. Jæger, Miroslav Kuchta, Kent-Andre Mardal, and Marie E. Rognes. 2017. A Cell-Based Framework for Numerical Modeling of Electrical Conduction in Cardiac Tissue. *Frontiers in Physics* 5 (2017), 48. https://doi.org/10.3389/fphy.2017.00048

[48] Jun Zhou, Wan Kan Chan, and Justin Schwartz. 2018. Modeling of Quench Behavior of YBa $_2$ Cu $_3$ O $_{7-\delta}$ Pancake Magnets and Distributed Temperature Sensing-based Quench Detection for Operating Temperature 30 K - 77 K. *IEEE Transactions on Applied Superconductivity* PP (10 2018), 1–1. https://doi.org/10.1109/TASC.2018.2874423